
Universiteit
Leiden
The Netherlands

Exploring the effects of magnetic fields on star formation in galaxies and the growth of dynamos

Ridkokasha, Ivan

Citation
Ridkokasha, I. (2024). *Exploring the effects of magnetic fields on star formation in galaxies and the growth of dynamos*.

Version:	Not Applicable (or Unknown)
License:	License to inclusion and publication of a Bachelor or Master Thesis, 2023
Downloaded from:	https://hdl.handle.net/1887/3764958

Note: To cite this publication please use the final published version (if applicable).

Exploring the effects of magnetic fields on star formation in galaxies and the growth of dynamos

THESIS

submitted in partial fulfillment of the
requirements for the degree of

MASTER OF SCIENCE
in
PHYSICS

Author :	Ivan Ridkokasha
Student ID :	s3556123
Supervisor :	Dr. M. Schaller
Second corrector :	Dr. S.P. Patil

Leiden, The Netherlands, June 20, 2024

Exploring the effects of magnetic fields on star formation in galaxies and the growth of dynamos

Ivan Ridkokasha

Instituut-Lorentz for Theoretical Physics, Leiden University
P.O. Box 9506, NL-2300 RA Leiden, The Netherlands

June 20, 2024

Abstract

Observations show that magnetic fields are present and dynamically important in all observed galaxies. It is now well established that these fields were amplified by the magnetic dynamo, although the details are still unclear. The only practical way to study complex setups like galaxy formation is through numerical simulations. However, including magnetic fields in simulations is a nontrivial task because of the unique solenoidal constraint $\boldsymbol{\nabla} \cdot \boldsymbol{B} = 0$.

In this thesis, we used a newly implemented smoothed-particle magnetohydrodynamics (SPMHD) with a divergence cleaning module in SWIFT. We run a galaxy formation in 'the cooling halo' and galaxy evolution in 'the isolated galaxy' setups, both without stellar feedback. Although SPMHD implementation was thoroughly tested on default tests, we found that it struggles with this setup. We conclude that the issues arise from the density contrast between the forming disk and halo. The divergence cleaning struggles to maintain a low divergence error and sometimes even increases it. This results in a spurious dynamo and, in some cases, a "numerical explosion" in internal and turbulent energies.

We find that having higher spatial and temporal resolution helps to resolve numerical issues. However, it makes computational cost unrealistic for larger cosmological runs. We propose ideas that can help to fix the problem without high computational cost – like a more aggressive timestep limiter near the problematic region with density contrast.

Finally, we find no dynamo in the runs without numerical issues.

Contents

Version of June 20, 2024– Created June 20, 2024 - 18:40

Chapter 1

Introduction

In the last few decades, our understanding of large-scale structure and galaxy formation has greatly improved. A lot of questions and mysteries were resolved, and now we are transitioning into a new era: the era of precision cosmology, where not only qualitatively correct but also quantitatively accurate predictions are crucial. A great part of this success can be attributed to the rapid development of cosmological simulations. Gravitational collapse quickly becomes nonlinear and analytically intractable. Additionally, various cooling mechanisms, star formation and stellar feedback complicate galaxy formation even more, leaving no hope of studying the process analytically. Numerical approaches, however, allow us to simulate such complicated environments and have become a reliable tool in structure formation over the last decades [1].

One of the aspects of galaxy formation that was included in the simulations only in the last 20-30 years is magnetic fields. From observations of galaxies, we measure relatively high magnetic fields that are dynamically important. One of the questions of interest is where these magnetic fields come from. In the last years, overwhelming evidence has been gathered supporting the dynamo mechanism – exponential amplification of the magnetic field using turbulent motion energy. Still, details of how exactly this mechanism produced observed magnetic fields are lagging with some discrepancies between theory and observations. These questions are hoped to be answered by simulations. However, simulating magnetic phenomena is hard, and the field is still young, with no consensus on how to do it and what results are correct or not [2].

In this thesis, we study the newly developed smoothed particle magnetohydrodynamics module inside the SWIFT code. And where dynamo results obtained with it lie among other observational, theoretical, and nu-

merical works.

1.1 Observational evidence of magnetic fields in galaxies

Magnetic fields are common in the universe at all scales. The Earth has magnetic field of 0.25 to 0.65 G on its surface (1 G = 10^{-4} T). The Sun has a magnetic field – usually around a few Gauss, but in sunspots, it can reach $\sim$ 2 kG, and even more, deeper in the convection zone. The strongest magnetic fields are believed to be in neutron stars, and they can reach 10^{13} to 10^{15} G (compare with the maximum produced by humans $\sim 10^{7}$ G). While the largest in scale observed magnetic fields are in galaxies and clusters of galaxies of 10 to 100 µG and 0.1 to 1 µG respectively. For more details, see review [3] and book [4].

1.1.1 Observational methods

In this project, we are especially interested in the magnetic fields in galaxies. Hence, let's discuss how magnetic fields in them are measured and what measurements tell us. Before that, it is important to note that the total magnetic field in a galaxy consists of a regular (has a well-defined direction at galactic scales) and a turbulent component (frequently reverses its direction). Different methods measure different projections of regular and/or turbulent components. For more details, see this review [5].

1. **Synchrotron Radiation**

   Ultra-relativistic cosmic ray particles emit electromagnetic radiation when they accelerate due to Lorentz force in the magnetic field. The intensity of the synchrotron radiation depends both on the magnetic field strength and number density of cosmic rays. To disentangle between the two, the expected equipartition of magnetic and cosmic rays' energy is used. This allows us to measure *strength of total field perpendicular to the line of sight* [6].

   Synchrotron radiation also has an intrinsic polarization that can help to *measure the direction of magnetic field and distinguish between turbulent and ordered component* [7].

2. **Faraday Rotation**

While polarized light travels in a magnetized plasma, its polarization angle rotates. The rotation angle is equal to $\Delta\chi = RM\lambda^2$, where λ is the observed wavelength, and RM is the rotation measure, which is equal to the integral along the line of sight: $RM = \int B_{||} n_e dl$. If we can estimate electron density, then by the polarization angle's dependence on the wavelength, one can measure *regular magnetic field component along the line of sight* [7].

Turbulent magnetic fields will wavelength-dependently decrease overall polarization, which is known as Faraday depolarization. By measuring this effect, one can find *turbulent magnetic field along the line of sight* [7].

3. **Dust Extinction/Emission Polarization**

   Elongated dust grains in the interstellar medium orient their minor axis along the mean magnetic field by the Davis-Greenstein effect or radiative torque alignment. They effectively form an anisotropic dust medium that emits polarized infrared light – with the polarization direction perpendicular to the mean magnetic field. Similarly, initially unpolarized starlight will become polarized in the direction parallel to the mean magnetic field after going through such dust.

   Therefore, by detecting the direction and degree of polarization in the infrared and optical ranges, one can measure *the direction and strength of the ordered field perpendicular to the line of sight* [8].

4. **Zeeman effect**

   This is the most direct way to measure magnetic fields – in magnetic fields, each emission spectral line splits into a few lines with different frequencies and polarizations. The frequency shift of each line is proportional to the magnetic field. However, for characteristic fields in galaxies, this effect is tiny and requires high line intensity and careful control of instrument polarization. Therefore, it has been used only for the Milky Way and starburst galaxies. It allows measuring *the strength of the regular field along the line of sight* [9].

1.1.2 Results of observational measurements

Using the aforementioned methods, many measurements of magnetic fields in galaxies have been performed. See [5] for a review. Here are some of the results:

Version of June 20, 2024– Created June 20, 2024 - 18:40

1. Assuming equipartition between magnetic energy and cosmic rays, the radio synchrotron emission measurements indicate that the average strength of total magnetic fields in spiral galaxies is $B_{\text{tot}} =$ 10 to 20 μG [10].

2. Even higher magnetic fields can be found in galaxies with high star formation, up to 100 μG [11].

3. From polarization of synchrotron emission, the average strength of ordered fields perpendicular to the line of sight is found to be around 5 to 10 μG with a ratio $B_{\text{ord},\perp}/B_{\text{tot}} = 0.3$. The direction of the magnetic fields forms a distinct spiral pattern (see Figure 1.1e) [10].

4. Total magnetic energy density is similar to the average kinetic energy density of the turbulent motions of the gas – so-called *equipartition*. This means that magnetic fields in galaxies are dynamically important. Still, magnetic energy density is $500 - 1000$ times smaller than the kinetic of the bulk rotation of the gas [12].

1.1.3 Evidence for dynamo action in galaxies

One of the central questions about magnetic fields in galaxies is of their origin. Historically, first was an idea of a large-scale primordial magnetic field that is then winded up in the galaxy following the matter [13, 14]. During the galaxy collapse, the magnetic field will be amplified due to the adiabatic contraption (2.9) and reach today's values of 1 to 10 μG. This idea is commonly termed the primordial origin of the magnetic field.

However, it is now firmly believed that current microgauss magnetic fields are not primordial but rather were significantly amplified by the magnetic dynamo. We discuss the dynamo mechanism in more detail in the following section 2.2 – it is a way for exponential amplifications of magnetic fields from the turbulent motion energy. Note the word "amplify" – dynamo cannot create a magnetic field, so some kind of seed field is still required. The origin of the seed field is pretty much an open question now – it could be of an astrophysical origin or primordial one.

Here, we discuss some of the differences between dynamo-amplified and primordial winding-up scenarios in galaxies and observational evidence for the former.

First, there is a topological difference in a final magnetic field in two scenarios (see Figure 1.1). Winding of primordial magnetic field will give bisymmetric spiral (Figure 1.1b) with odd symmetry (1.1d) in the vertical

Version of June 20, 2024– Created June 20, 2024 - 18:40

direction with tiny pitch angle $\lesssim 1^\circ$ (1.1f). In large-scale dynamos, however, the dominant mode is an axisymmetric spiral (1.1a) with even symmetry in the vertical direction (1.1c) with a pitch angle around 20° (1.1e). See reviews [2, 3] for more details.

Observations support the dynamo picture on all three points. Faraday rotations measurements show that in most of the galaxies, axisymmetric mode is dominant, while bisymmetric is present only in a few [10]. In the Milky Way, it was possible to measure vertical symmetry, and it is even [15]. Finally, measured ordered magnetic fields make a trailing spiral with a pitch angle in the range $10^\circ - 30^\circ$ [16].

Second, the measured strength of the magnetic fields is close to the energy equipartition with turbulent motions. Such equipartition is directly predicted in the dynamo model, while there is nothing similar for the primordial magnetic fields hypothesis [16].

There is also a tight radio-IR correlation that suggests that the total magnetic field is correlated to the star formation rate: $B_{\rm tot} \propto \Sigma_{\rm SFR}^{0.30}$. This is again a sign of dynamo action – how turbulence from stellar feedback translates into magnetic fields [17].

1.2 Simulations of magnetic fields in galaxies

Simulating magnetic fields is a nontrivial task since the chosen discretization of the magnetic field should obey its unique solenoidal constraint $\boldsymbol{\nabla} \cdot \boldsymbol{B} = 0$.

In Eulerian codes (with either constant or moving mesh), it is possible to ensure this using the constrained transport scheme [19]. In this scheme, magnetic fields are defined per each cell surface instead of the usual volume averaged per cell. Then, by keeping the total flux of the magnetic field through the surfaces of each cell equal to zero, one automatically ensures $\boldsymbol{\nabla} \cdot \boldsymbol{B} = 0$ according to the divergence theorem.

However, for galaxy formation, Lagrangian codes are usually used (like mesh-free smoothed-particle hydrodynamics) since they have inherent spatial adaptability. For Lagrangian approaches, there are no alternatives like constrained transport. Therefore, they rely on divergence cleaning algorithms [20, 21]. Although divergence cleaning is stable, it can lead to numerical artefacts, and some of them can mimic dynamo [22]. We discuss examples of problems throughout the thesis since we also use the Lagrangian approach with the Dedner divergence cleaning.

There are two types of dynamos in galaxies – small-scale, occurring at turbulent scales 10 to 100 pc and creating turbulent magnetic fields; and

Version of June 20, 2024– Created June 20, 2024 - 18:40

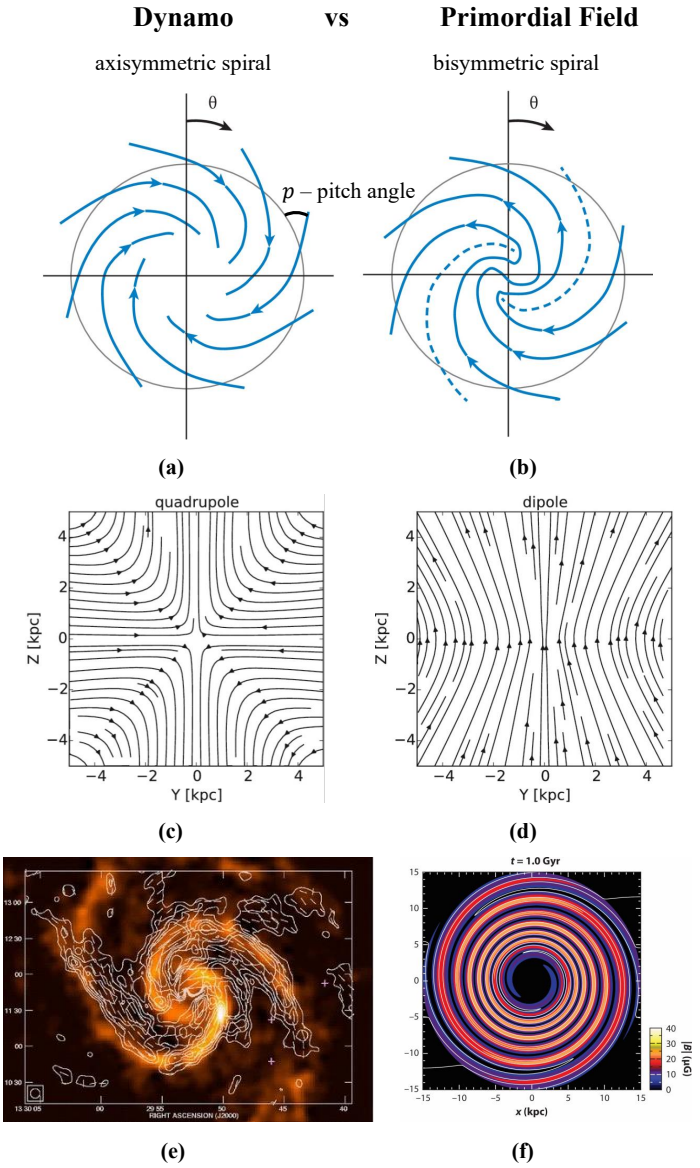

Figure 1.1: *Comparison of magnetic field topology between dynamo generated (left column) and winded-up primordial fields (right column). (a, b) In-plane fields: dynamo generates axisymmetric spiral while winding up – bisymmetric. Also, figure (a) illustrates the definition of the pitch angle – the angle between a spiral and the corresponding circle. (c, d) Vertical component: dynamo generates quadrupole field with even symmetry along z, while primordial fields will likely wind up as a dipole with odd symmetry. (e) Polarized radio emission (contours) and B-vectors of M51 superimposed on the colour image of the CO line emission from molecular gas. The observed pitch angle is $p = 20°$. (f) Simulation of winding up of the primordial field during galaxy formation. The pitch angle is $p = 3°$. Figures (a, b, f) are taken from [2], figures (c, d) from [18], and figure (e) from [5].*

large-scale, producing ordered fields at the scale of the galaxy.

Currently, there is no consensus in the field of galactic dynamo simulations. Different papers disagree on what drives dynamos, their rate and equipartition value, or even if the dynamos we see in simulations resemble physical or purely numerical artefacts. Nevertheless, most simulations show that both small and large-scale dynamo operate simultaneously and resolving both is essential to understanding galaxy formation [2].

Analytical estimates and observational evidence suggest that turbulence created by supernova explosions is one of the main drivers of small-scale dynamos. However, some of the simulations were done without including supernova explosions and still show rapid amplification (much faster than expected from pure large-scale dynamo) [23, 24]. Moreover, some papers show small or no difference between runs with or without supernova feedback [25, 26]. At the same time, other simulations show that indeed, without supernova-driven turbulence, there is only moderate amplification [27, 28] or no dynamo at all [18, 29]. This discrepancy is likely because most simulations do not have enough resolution to capture small-scale turbulent dynamics, but it may also indicate spurious dynamos in some magnetohydrodynamics (MHD) schemes.

Observations show that magnetic field energy is close to the equipartition with the turbulent. Simulations also disagree on this front: some show that magnetic energy can reach and even overshoot turbulent and internal energies [23, 30], while in others, it only reaches a fraction of turbulent energy [31]. Some of the authors suggest that this difference could be because of the different MHD schemes [22].

Finally, the dynamo growth rate – in all of the papers that study dynamos in the isolated galaxy, it changes with the resolution, meaning that the dynamo is not resolved. Moreover, rates vary within different setups and MHD schemes [22].

In conclusion, one should be very careful when selecting an MHD scheme, especially in how it handles solenoidal conditions and be cautious in the analysis to distinguish any numerical artefacts and physics.

Chapter 2

Theory

2.1 The equations of magnetohydrodynamics

In SI units, Maxwell's equations can be written in the form:

$$\boldsymbol{\nabla} \cdot \boldsymbol{E} = \frac{\rho}{\epsilon_0} \tag{2.1}$$

$$\boldsymbol{\nabla} \cdot \boldsymbol{B} = 0 \tag{2.2}$$

$$\frac{\partial \boldsymbol{B}}{\partial t} = -\boldsymbol{\nabla} \times \boldsymbol{E} \tag{2.3}$$

$$\frac{1}{c^2}\frac{\partial \boldsymbol{E}}{\partial t} = \boldsymbol{\nabla} \times \boldsymbol{B} - \mu_0 \boldsymbol{J}. \tag{2.4}$$

To get a standard magnetohydrodynamics (MHD) equation, we also add the standard Ohm's law:

$$\boldsymbol{J} = \sigma(\boldsymbol{E} + \boldsymbol{U} \times \boldsymbol{B}), \tag{2.5}$$

where $\boldsymbol{U}$ is a velocity of the gas and σ is its electric conductivity. Instead of σ, magnetic diffusivity is often used $\eta = (\mu_0\sigma)^{-1}$ (in cgs units $\eta = c^2/(4\pi\sigma)$ and often called resistivity). Then, substituting Ohm's law (2.5) into (2.4):

$$\left(\frac{1}{\eta} + \frac{1}{c^2}\frac{\partial}{\partial t}\right)\boldsymbol{E} = \left(\frac{1}{\eta}\boldsymbol{U} - \boldsymbol{\nabla}\right) \times \boldsymbol{B}. \tag{2.6}$$

In all the astrophysics problems, the relevant timescale over which the electric field varies is orders of magnitudes larger than Faraday time $\tau_{\text{Faraday}} = \eta/c^2$. Hence, the time derivative of $\boldsymbol{E}$ can be neglected. Going back to the equation (2.4), we can now rewrite it as Ampere's law:

$$\boldsymbol{J} = \frac{1}{\mu_0}\boldsymbol{\nabla} \times \boldsymbol{B}. \tag{2.7}$$

Now, by substituting Ohm's law (2.5) into Faraday's law (2.3) and using Ampere's law (2.7), one can get a single evolution equation for $\boldsymbol{B}$:

$$\frac{\partial \boldsymbol{B}}{\partial t} = \boldsymbol{\nabla} \times (\boldsymbol{U} \times \boldsymbol{B}) - \eta \boldsymbol{\nabla} \times (\boldsymbol{\nabla} \times \boldsymbol{B})$$

or using curl of curl identity and Gauss's law (2.2):

$$\frac{\partial \boldsymbol{B}}{\partial t} = \boldsymbol{\nabla} \times (\boldsymbol{U} \times \boldsymbol{B}) + \eta \boldsymbol{\nabla}^2 \boldsymbol{B}. \tag{2.8}$$

This equation is called **the induction equation**.

Now, let's discuss its properties. The first term on the right-hand side $\boldsymbol{\nabla} \times (\boldsymbol{U} \times \boldsymbol{B})$ correspond to changes in the magnetic field due to the movement of the fluid. More generally, this term implies that the magnetic flux through a surface moving with the fluid remains constant – this effect is also called **flux freezing**.

One example of this effect is magnetic field amplification due to adiabatic contraption. During the spherical collapse, all the surface areas will shrink, and the magnetic field will get amplified. Since $B \sim 1/S \sim 1/l^2$ and density is $\rho \sim 1/l^3$ during such collapse, the magnetic field will get amplified as

$$B = B_0 \left(\frac{\rho}{\rho_0} \right)^{2/3}, \tag{2.9}$$

where B_0 and ρ_0 are initial values.

Second term $\eta \boldsymbol{\nabla}^2 \boldsymbol{B}$ corresponds to the diffusion of the magnetic field. Diffusivity varies a lot with temperature and whether or not gas is ionized (for more details, see [3]). For galaxies, typical diffusivity is very small $\eta \sim 10^7\,\mathrm{cm^2 s^{-1}}$. This means that diffusion even on a scales of 1 AU will take $\sim 1000\,\mathrm{Gyr}$.

To have a full system of evolution equations, one should also couple the induction equation (2.8) with the momentum equation. It is the usual Navier-Stokes equation with additional Lorentz force $\boldsymbol{J} \times \boldsymbol{B}$. In simplification of incompressible fluid:

$$\frac{\mathrm{D}\boldsymbol{U}}{\mathrm{D}t} = -\frac{1}{\rho} \boldsymbol{\nabla} p + \frac{\boldsymbol{J} \times \boldsymbol{B}}{\rho} + \boldsymbol{f} + \nu \boldsymbol{\nabla}^2 \boldsymbol{U}, \tag{2.10}$$

where $\mathrm{D}/\mathrm{D}t = \partial/\partial t + \boldsymbol{U} \cdot \boldsymbol{\nabla}$ is the Lagrangian derivative, ν is kinematic viscosity, $\boldsymbol{f}$ is external force per unit mass (gravity, for instance).

For some considerations, it is useful to rewrite Lorentz force as

$$\boldsymbol{J} \times \boldsymbol{B} = \frac{1}{\mu_0} (\boldsymbol{\nabla} \times \boldsymbol{B}) \times \boldsymbol{B} = \frac{(\boldsymbol{B} \cdot \boldsymbol{\nabla}) \boldsymbol{B}}{\mu_0} - \boldsymbol{\nabla} \left(\frac{\boldsymbol{B}^2}{2\mu_0} \right), \tag{2.11}$$

Version of June 20, 2024– Created June 20, 2024 - 18:40

where the first term is called **magnetic tension** and acts to straighten magnetic field lines, and the second term is the **magnetic pressure** force that opposes the build-up of high magnetic energies.

2.2 Basic dynamo theory

General dynamo theory is very complicated since it requires solving a nonlinear set of equations (2.8) and (2.10). Up to the 1950s, it was generally believed that magnetic dynamo was impossible. Only after pioneering theoretical works of Parker, Backus, Herzenberg, Roberts [32–35] and experiments of Lowes & Wilkinson [36], people start taking the possibility of dynamos seriously.

There are at least two requirements for any known dynamo:

- It requires three dimensions. In two dimensions, there is no dynamo (antidynamo theorem [37]).
- It requires nonzero resistivity $\eta \neq 0$. For some dynamo mechanisms, only small resistivity is required ($\eta \to 0$).

Dynamos are divided into two types: small-scale and large-scale dynamos. Small-scale dynamo operates on characteristic turbulent scales and usually generates turbulent magnetic fields, while large-scale dynamo is responsible for ordered magnetic fields correlated on larger scales.

Let's start with small-scale dynamo. A nice example to understand the overall mechanism is the so-called stretch-twist-fold (STF) dynamo. Figure 2.1 illustrates the mechanism. A key to this mechanism is flux freezing (section 2.1) – conservation of magnetic flux through a surface moving with the fluid.

In this mechanism, we consider a "rope" of incompressible fluid with magnetic flux along it. First (stretch, $A \to B$), the rope is stretched to twice its length. Since volume is conserved, the rope's cross-section becomes two times smaller, and the magnetic field doubles. This is the part where magnetic energy is amplified from the turbulent kinetic energy. Second, (twist, $B \to C$) the rope is twisted into figure eight – this part requires a third dimension. Then, (fold, $C \to D$) the rope is folded so that there are two loops, each with doubled the magnetic field and half the cross-section. Finally (merge, $D \to A$), to save this state and avoid future turbulent disentanglement, two circles merge due to magnetic diffusion. This part requires nonzero resistivity, although it can be relatively small.

Version of June 20, 2024– Created June 20, 2024 - 18:40

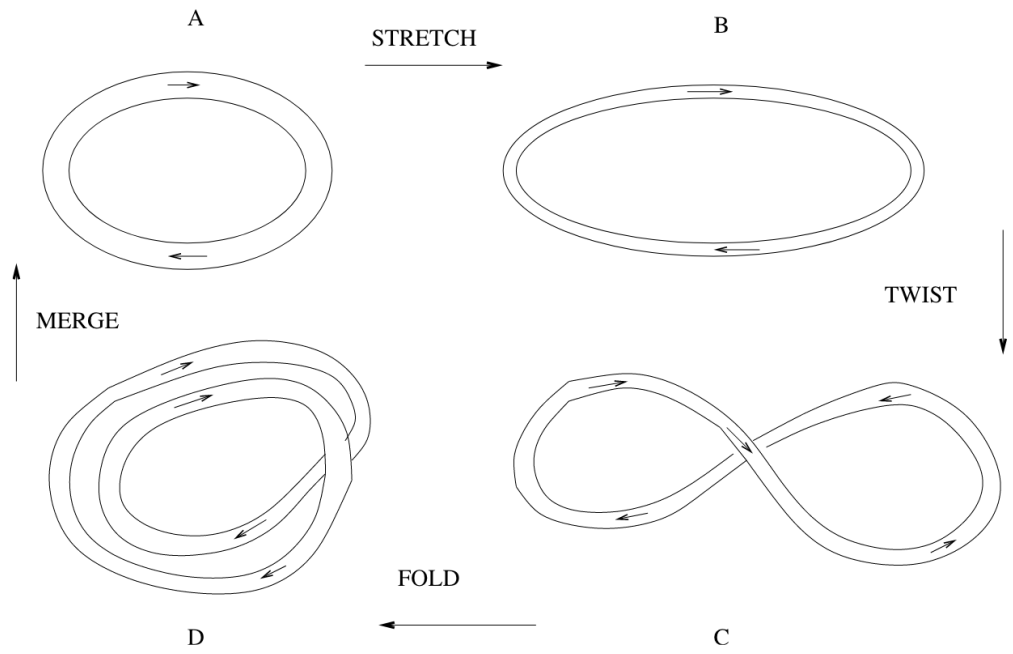

Figure 2.1: *A schematic illustration of the stretch-twist-fold dynamo. The Figure is taken from [3].*

This way, the magnetic field is doubled. Repeating this mechanism n times, we get 2^n amplification. If one STF cycle takes around T time, this mechanism gives exponential growth with $T^{-1} \ln 2$ growth rate.

When the magnetic field increases up to dynamically important values, it may limit the efficiency of the dynamo. Namely, magnetic curvature forces may limit the twist part, or magnetic pressure may break down the incompressibility assumption and not allow the cross-section to shrink and increase the magnetic field. When this happens, dynamo **saturates** and magnetic field stop growing.

A more detailed analytical theory of small-scaled dynamos is also possible and was done first by Kazantsev [38]. For more details, see [3]. Here we note the following: small-scale dynamos should operate in galaxies driven by turbulence from supernova explosions; small-scale dynamo rate is estimated to increase magnetic field up to microgauss levels in $\sim 10^8$ years; small-scale dynamo saturates at equipartition with the turbulent energy [23, 39, 40].

Small-scale dynamos play a significant role in galaxies – they are primarily responsible for quickly increasing tiny seed fields up to microgauss values. However, small-scale dynamos cannot explain large spiral pat-

Version of June 20, 2024– Created June 20, 2024 - 18:40

terns in magnetic fields. For this, we need *a large-scale dynamo*.

For large-scale dynamo, we can use mean-field treatment, averaging the effective action of the turbulence on large scales. Then in the mean-field treatment equation (2.8) can be rewritten as

$$\frac{\partial \overline{\boldsymbol{B}}}{\partial t} = \boldsymbol{\nabla} \times \left(\overline{\boldsymbol{U}} \times \overline{\boldsymbol{B}} + \overline{\boldsymbol{\mathcal{E}}} - \eta \overline{\boldsymbol{J}} \right), \tag{2.12}$$

where $\overline{\boldsymbol{B}}$, $\overline{\boldsymbol{U}}$ are mean field values, η – is effective diffusivity due to turbulent flows, and $\overline{\boldsymbol{\mathcal{E}}} = \overline{\boldsymbol{u} \times \boldsymbol{b}}$ is averaged electromotive force. Electromotive force is then assumed to be approximated by $\overline{\boldsymbol{\mathcal{E}}} \approx \alpha \boldsymbol{B}$, where α is some pseudoscalar in the setup. The simplest pseudoscalar that occurs in galaxies is the scalar product of some gradient ($\boldsymbol{g}$ vector) and angular velocity ($\boldsymbol{\Omega}$ pseudovector) $\alpha \sim \boldsymbol{g} \cdot \boldsymbol{\Omega}$. In galaxies, this gradient could be of density or turbulent velocity.

The first mechanism of large-scale amplification in galaxies – is the Ω effect. This is an efficient way to amplify the toroidal field from the poloidal, from shear (differential rotation). To have a full exponential growth, also efficient way to amplify the poloidal field back from toroidal is needed. This is done by electromotive force $\overline{\boldsymbol{\mathcal{E}}} \approx \alpha \boldsymbol{B}$ and called the α effect.

Combined, this mechanism is called α-Ω dynamo and is believed to be the main source of large-scale spiral fields in galaxies (see Figure 2.2 for illustration).

2.3 Evolution of magnetic fields in galaxies

As discussed in the section 1.1.3, observations suggest that dynamo plays a central role in the evolution of magnetic fields in galaxies. Moreover, we observe both turbulent and ordered fields and from theoretical estimates, it follows that both small and large-scale dynamos operate in galaxies.

In this picture evolution of magnetic fields consists of three stages: (1) seeding, (2) amplifying, (3) ordering and sustaining.

- To operate, dynamo requires an initial (so-called seed) field. This seed field can be either primordial (generated during inflation or one of the phase transitions in the early universe) or of astrophysical origin. There are various astrophysical mechanisms that explain how to create a non-zero electric current from zero one. Usually, they use the fact that negative charges (electrons) are much lighter than positive charges (protons) in the universe. Therefore, applying pressure

Version of June 20, 2024– Created June 20, 2024 - 18:40

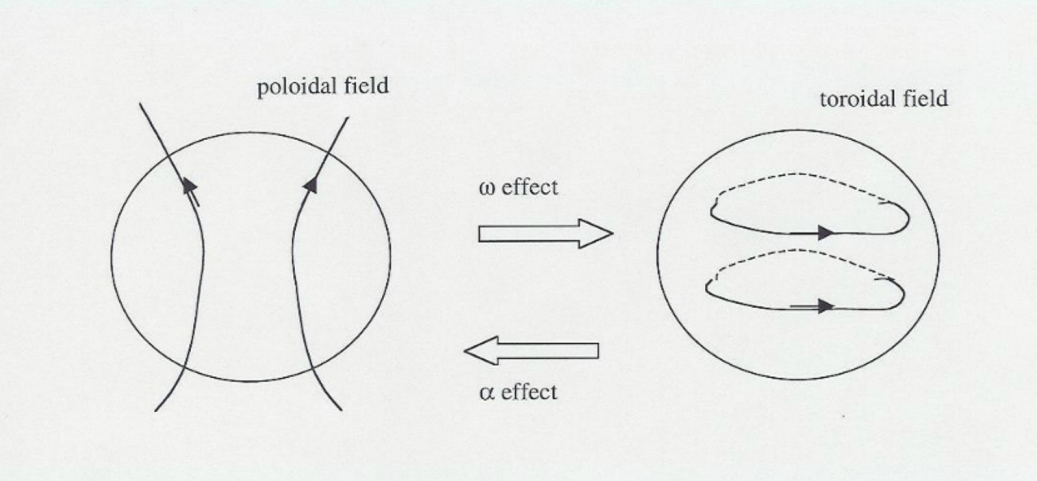

Figure 2.2: *A schematic illustration of the large-scale α-Ω dynamo. The Figure is taken from [41].*

or temperature gradient will accelerate different charges differently and generate electrical current and magnetic fields (see, for example, Biermann battery [42]).

- An efficient way to amplify the magnetic field is a small-scale dynamo that operates in a turbulent gas generated by supernova explosions or spiral shocks. It can amplify seed field to the μG values in $\sim 1 \times 10^8$ yr. The resulting field is turbulent and in equipartition with the turbulent energy of the galaxy.
- Finally, galactic magnetic fields get ordered at larger scales, presumably by $\alpha - \Omega$ dynamo (Figure 2.2). This process is the most time-consuming and takes a few Gyr to generate large-scale ordered fields with spiral patterns (see Figure 1.1e).

Chapter 3

Simulation methods

3.1 The gravity and hydrodynamics code SWIFT

To simulate galactic magnetic fields, we use SWIFT [43] – a fully open-source coupled cosmology, gravity, hydrodynamics, and now also magnetohydrodynamics code.

In this project, we will simulate only gravitationally bounded objects; therefore, we ignore the cosmological expansion of the universe.

Self-gravity on short ranges is computed using the Fast Multipole Method, and on large ranges using the particle-mesh method solved in Fourier space. At the same time, in SWIFT, many external gravitational potentials are implemented. In this project, we use both self-gravity and external potential.

For the hydrodynamics, SWIFT uses a smoothed-particle hydrodynamics (SPH) scheme. It is a mesh-free Lagrangian method, where the fluid is divided into discrete moving "particles" with assigned mass, velocity, temperature, etc. Then, any simulated quantity at any other point can be interpolated from the nearby particles' values using the given kernel. In this project, we use Wendland C2 kernel [44] with the resolution parameter $\eta = 1.2348$, which corresponds to 58 weighted neighbours considered in each interpolation. The width of the kernel for each particle is defined by the smoothing length h, which is adaptively recalculated.

Then, one can rewrite continuous evolution equations of fluid dynamics into discrete ones for the particles. Specifically, we use the SPHENIX SPH scheme [45], designed for galaxy formation problems. The SPHENIX scheme uses a density-energy formulation of the equations of motion combined with artificial viscosity and conduction terms to capture shocks.

Equations are also discrete in time. To solve them, SWIFT uses the stan-

dard leapfrog method with the individual time-step of the particles set as a minimum of gravity time-step, hydrodynamics Courant-Friedrichs-Lewy (CFL) condition and similar conditions for magnetohydrodynamics. Also, we run simulations with a time-step limiter inspired by [46] that limits the difference in time-step in nearby particles to better conserve energy and momentum in violent events.

3.2 Smoothed-particle magnetohydrodynamics

Similarly, one can apply a smoothed-particle scheme to rewrite MHD equations 2.8 and 2.10. In this project, we consider only ideal MHD – when $\eta = 0$ and $\nu = 0$. Then, induction and momentum equations can be rewritten in the following form:

$$\frac{\mathrm{D}}{\mathrm{D}t}\left(\frac{\boldsymbol{B}}{\rho}\right) = \left(\frac{\boldsymbol{B}}{\rho}\cdot\boldsymbol{\nabla}\right)\boldsymbol{u}, \tag{3.1}$$

$$\frac{\mathrm{D}u^i}{\mathrm{D}t} = -\frac{1}{\rho}\frac{\partial S^{ij}}{\partial x^j}, \tag{3.2}$$

$$S^{ij} = (P + \frac{\boldsymbol{B}^2}{2\mu_0})\delta^{ij} - \frac{B^i B^j}{\mu_0},$$

where S^{ij} is a Maxwell stress tensor.

One can discretize these equations on "particles" by assigning each particle a magnetic field (or, more precisely, magnetic field over density $\boldsymbol{B}/\rho$). This scheme is called SPMHD – smoothed-particle magnetohydrodynamics and was first implemented by [47]. In our group, a similar module for SWIFT was done by O Karapiperis, FA Stasyszyn, N Shchutskyi, and M. Schaller.

However, straightforward discretization of the MHD equation onto the SPH scheme can lead to problems. Mainly because of solenoidal constraint that is never directly enforced. To fix it, special "MHD tricks" are introduced. In the current SWIFT implementation, all the tricks are similar to the PHANTOM [48].

3.2.1 Tensile instabilities

Induction and momentum equations in the form (3.1), (3.1) conserve energy and momentum for any magnetic fields. However, when $\boldsymbol{\nabla}\cdot\boldsymbol{B}$ is not zero, these equation creates unphysical forces that can lead to tensile instabilities: particles can start to attract each other in high magnetic fields.

Version of June 20, 2024– Created June 20, 2024 - 18:40

This problem is solved by adding additional force on the particle $f^i_{\text{divB}} = -\frac{B^i}{\rho}(\boldsymbol{\nabla} \cdot \boldsymbol{B})$ that cancels the unphysical part.

This force, however, leads to momentum and energy non-conservation. Therefore, it is applied only where necessary, namely where magnetic pressure is at least 0.1 of thermodynamic pressure.

3.2.2 Artificial resistivity

Second, because of finite resolution, pure SPH does not correctly capture discontinuities, like shocks from supernovae. To fix this, one can add artificial viscosity (for discontinuities in velocity) and artificial conduction of energy (for discontinuities in temperature). Similarly, in SPMHD, artificial resistivity is added to the equations (3.1), (3.2) to capture discontinuities in the magnetic field. It acts similarly to the physical resistivity, removing energy from the magnetic field to the internal energy as $\eta \boldsymbol{\nabla}^2 \boldsymbol{B}$, where artificial resistivity η is decreasing with higher resolution.

3.2.3 Dedner cleaning

The most important problem with SPMHD scheme is that solenoidal constraint $\boldsymbol{\nabla} \cdot \boldsymbol{B} = 0$ is never directly enforced. Because of numerical errors divergence will grow leading to unphysical results. In current implementation this problem is solved using constained Dedner cleaning [21, 49, 50].

Main idea of the cleaning is to propagate divergence error according to dumped wave equation:

$$\frac{\partial^2(\boldsymbol{\nabla} \cdot \boldsymbol{B})}{\partial t^2} - c_h^2 \boldsymbol{\nabla}^2(\boldsymbol{\nabla} \cdot \boldsymbol{B}) + \frac{1}{\tau_c}\frac{\partial(\boldsymbol{\nabla} \cdot \boldsymbol{B})}{\partial t} = 0. \tag{3.3}$$

This is achieved by introducing a new scalar field (dedner scalar ψ) that is coupled to the magnetic field through additional term in the induction equation

$$\frac{\mathrm{D}}{\mathrm{D}t}\left(\frac{\boldsymbol{B}}{\rho}\right) = -\frac{1}{\rho}\boldsymbol{\nabla}\psi. \tag{3.4}$$

The scalar is evolved according to

$$\frac{\mathrm{D}}{\mathrm{D}t}\left(\frac{\psi}{c_h}\right) = -c_h \boldsymbol{\nabla} \cdot \boldsymbol{B} - \frac{1}{2c_h}\psi \boldsymbol{\nabla} \cdot \boldsymbol{U} - \frac{\psi}{\tau_c c_h}, \tag{3.5}$$

where c_h is a cleaning speed, set to the fast magnetosonic speed:

$$c_h = \sqrt{c_s^2 + \frac{\boldsymbol{B}^2}{\mu_0 \rho}}, \tag{3.6}$$

Version of June 20, 2024– Created June 20, 2024 - 18:40

where c_s is a speed of sound.

Decay time is set by

$$\tau_c = \frac{h}{c_h},$$

where h – is a smoothing length of a particle as defined by kernel, approximately equal to the interparticle distance.

To keep track of the divergence usual metric is dimensionless divergence error:

$$\epsilon_{\mathrm{divB}} = \frac{h|\boldsymbol{\nabla} \cdot \boldsymbol{B}|}{|\boldsymbol{B}|}. \tag{3.7}$$

A rule of thumb is to keep this error below $\lesssim 10^{-2}$.

3.2.4 Time-stepping

MHD involved in time-stepping in two places. First, it changes signal velocity v_{sig} in the standard hydrodynamics CFL condition from simple sound speed to the fast magnetosonic speed (3.6):

$$\Delta t_{\mathrm{hydro}} = C_{\mathrm{CFL}} \frac{h}{v_{\mathrm{sig}}},$$

where CFL constant $C_{\mathrm{CFL}} = 0.075$ by default.

Second, there is a time-step related to the solenoidal constraint $\boldsymbol{\nabla} \cdot \boldsymbol{B} = 0$ which purpose is to better resolve dedner cleaning in particles with large divergence error:

$$\Delta t_{\mathrm{MHD}} = C_{\mathrm{CFL}} \sqrt{\frac{\rho \mu_0}{(\boldsymbol{\nabla} \cdot \boldsymbol{B})^2}}. \tag{3.8}$$

Version of June 20, 2024– Created June 20, 2024 - 18:40

Chapter 4

Runs

In this project, we are especially interested in simulating galaxies and their formation. For a similar analysis of the magnetic fields in galaxy formation, but with other codes, see also [18, 23, 30, 31, 51]. The simplest setup to study is a single halo that starts to collapse. There is already a prepared example in SWIFT for that purpose – `CoolingHaloWithSpin`. To check some numerical issues, we also tried to simulate an already collapsed halo with a formed disk of gas and star particles – `IsolatedGalaxy`. First, let's describe those setups with default parameters we run them.

4.1 Simulation setups

4.1.1 Cooling halo with spin

This setup is one of the defaults in SWIFT. It considers a rotating isothermal ($T = \text{const}$) gas cloud in equilibrium inside a nonsingular isothermal sphere potential.

Since it is already a gravitationally bound object, the expansion of the universe does not have a large impact on it. So we ignore it.

Dark matter is static in this simulation and only provides external potential for the gas to evolve inside it. Potential Φ is fully specified by the rotational speed v_{rot} and softening length ε:

$$\Phi(r) = \frac{v_{\text{rot}}^2}{2} \ln(r^2 + \varepsilon^2). \tag{4.1}$$

The main purpose of softening length is to avoid numerical divergence in the centre; therefore, we take it small $0.1 - 1.0\,\text{kpc}$ and generally neglect it in theoretical estimates.

Neglecting ε, potential (4.1) corresponds to the following density distribution

$$\rho(r) = \frac{v_{\text{rot}}^2}{4\pi G r^2}. \tag{4.2}$$

From it, we can calculate the halo virial radius, the radius within which the average density of the halo $\langle \rho(r_{200}) \rangle = \frac{M_{200}}{\frac{4}{3}\pi r_{200}^3} = \frac{3v_{\text{rot}}^2}{4\pi G r_{200}^2}$ is 200 times larger than the mean matter density of the universe $\rho_m = \frac{3H^2}{8\pi G}\Omega_m$:

$$r_{200} = \frac{v_{\text{rot}}}{10H\sqrt{\Omega_m}}. \tag{4.3}$$

Similarly, one can calculate halo virial mass:

$$M_{200} = \frac{v_{\text{rot}}^2}{G} r_{200}. \tag{4.4}$$

Initially, the gas cloud is distributed in the hydrodynamic equilibrium with the gravitational potential from the dark matter, which corresponds to the following density and temperature:

$$\rho_{\text{gas}}(r) = \frac{\Omega_b}{\Omega_m} \frac{v_{\text{rot}}^2}{4\pi G r^2}. \tag{4.5}$$

$$T_{\text{eq}} = \frac{\mu v_{\text{rot}}^2}{2R} = \text{const.} \tag{4.6}$$

Without anything else, this configuration will stay in equilibrium. To see a galaxy formation, we need cooling – we start by considering simple constant lambda cooling:

$$\frac{du}{dt} = -\Lambda n_H^2, \tag{4.7}$$

where u – internal energy density, n_H – hydrogen density, and Λ – cooling rate, that we set to a typical value in galaxies $\Lambda = 10^{-23}\,\text{erg} \cdot \text{cm}^3/\text{s}$.

Now, the dense centre quickly cools down and collapses – forming a galaxy.

To have a disk in the galaxy, we also add rotation, which is specified by the dimensionless spin parameter:

$$\lambda = \frac{J|E|^{1/2}}{G M_{200}^{5/2}}, \tag{4.8}$$

where J is the total angular momentum of the halo inside the virial radius. We assume initial rotation along the z-axis with angular velocity inversely

Version of June 20, 2024– Created June 20, 2024 - 18:40

proportional to the radius:

$$\omega(r) = \frac{3J}{M_{200} r_{200}} \frac{1}{r}. \tag{4.9}$$

Finally, we also need a seed magnetic field to see its impact on the galaxy. If it is small enough, the initial configuration does not matter for future dynamo amplification (see, for example, [18, 30]. Therefore, we set $B_0 = 10^{-10}$ G uniform magnetic field, usually along x or z-axis.

To summarize, this example is fully defined by setting the following parameters:

1. Cosmological parameters: Hubble constant H, matter and baryon density parameters Ω_m, Ω_b, helium fraction X_{He}.
2. Halo mass M_{200} (or equivalently, rotational speed $v_{\rm rot}$) and softening length ε.
3. Cooling rate Λ.
4. Dimensionless spin parameter λ.
5. Seed magnetic field direction and value B_0.

Default parameters

Most of the tests performed in this section were done starting with the following simplest setup, also the default in `SWIFT` example of `CoolingHaloWithSpin`.

Code configuration

```
--with-ext-potential=isothermal
--with-cooling=const-lambda
--with-spmhd=direct-induction
--with-kernel=wendland-C2
--disable-hand-vec
```

Running flags

```
--external-gravity --cooling --hydro
--limiter --sync
```

Halo parameters

1. $H = 67.7\,\mathrm{kms}^{-1}\mathrm{Mpc}^{-1}$, $\Omega_m = 0.3$, $\Omega_b = 0.06$, $X_{He} = 0.248$;
2. $v_{\rm rot} = 200\,\mathrm{km/s}$ (this corresponds to $M_{200} = 5 \times 10^{12}\,\mathrm{M}_\odot$, $r_{200} = 540\,\mathrm{kpc}$, $T_{\rm eq} = 1.4 \times 10^6\,\mathrm{K}$) and softening length $\varepsilon = 1.0\,\mathrm{kpc}$;

3. $\Lambda = 10^{-23}\,\mathrm{erg}\cdot\mathrm{cm}^3/\mathrm{s}$;
4. $\lambda = 0.05$;
5. $B_0 = 10^{-10}\,\mathrm{G}$ along x-axis.

Numerical details

1. Resolution: 2900 gas particles inside the virial radius, each with a mass $87 \times 10^6\,\mathrm{M}_\odot$;
2. Full simulation is in a cubic box $4r_{200} \times 4r_{200} \times 4r_{200}$ with periodic boundary conditions;
3. CFL constant $C_{\mathrm{CFL}} = 0.075$;
4. Minimal allowed temperature $T_{min} = 10^4\,\mathrm{K}$.

4.1.2 Isolated galaxy

To test some numerical issues, we also tried `IsolatedGalaxy` example. It is a product of the cooling halo collapse that has an already-formed disk with gas particles and stars. It is also one of the defaults in SWIFT.

More specifically, it is a thin disk with $\sim 20\,\mathrm{kpc}$ radius and $\sim 1\,\mathrm{kpc}$ total height. There are no particles outside the disk, and the disk is far away from the boundaries of the box.

Initialy there are 25000 gas particles each of mass $6.576 \times 10^5\,\mathrm{M}_\odot$ and 113000 star particles: 84000 of masses $4.603 \times 10^5\,\mathrm{M}_\odot$ and 29000 of masses $6.576 \times 10^5\,\mathrm{M}_\odot$. Total gas mass is $1.6 \times 10^{10}\,\mathrm{M}_\odot$, which is ~ 4 times smaller than total stellar mass of $5.8 \times 10^{10}\,\mathrm{M}_\odot$.

Initial conditions are set to the Hernquist potential, and we simulate the galaxy inside one too. Hernquist potential is defined as

$$\Phi(r) = -\frac{GM_{200}}{r+a}, \tag{4.10}$$

where M_{200} is a halo mass, and a is a scale radius. In our setup $M_{200} = 1.37 \times 10^{12}\,\mathrm{M}_\odot$ and $a = 50\,\mathrm{kpc}$.

For simplicity and to compare the isolated galaxy with the cooling halo, we start by running a very similar setup. We also run it without star formation, with constant lambda cooling $\Lambda = 10^{-23}\,\mathrm{erg}\cdot\mathrm{cm}^3/\mathrm{s}$, temperature floor $T_{min} = 10^4\,\mathrm{K}$, and uniform seed field $B_0 = 10^{-10}\,\mathrm{G}$ along x-axis. The only significant difference is in gravity. While the cooling halo is simulated inside isothermal external potential without self-gravity, isolated galaxy, we simulate inside Hernquist potential with self-gravity included to match the initial conditions.

Version of June 20, 2024– Created June 20, 2024 - 18:40

4.2 Runs without magnetic fields

First, let's run the described setups without any magnetic fields to see the difference after adding magnetism.

4.2.1 Cooling halo

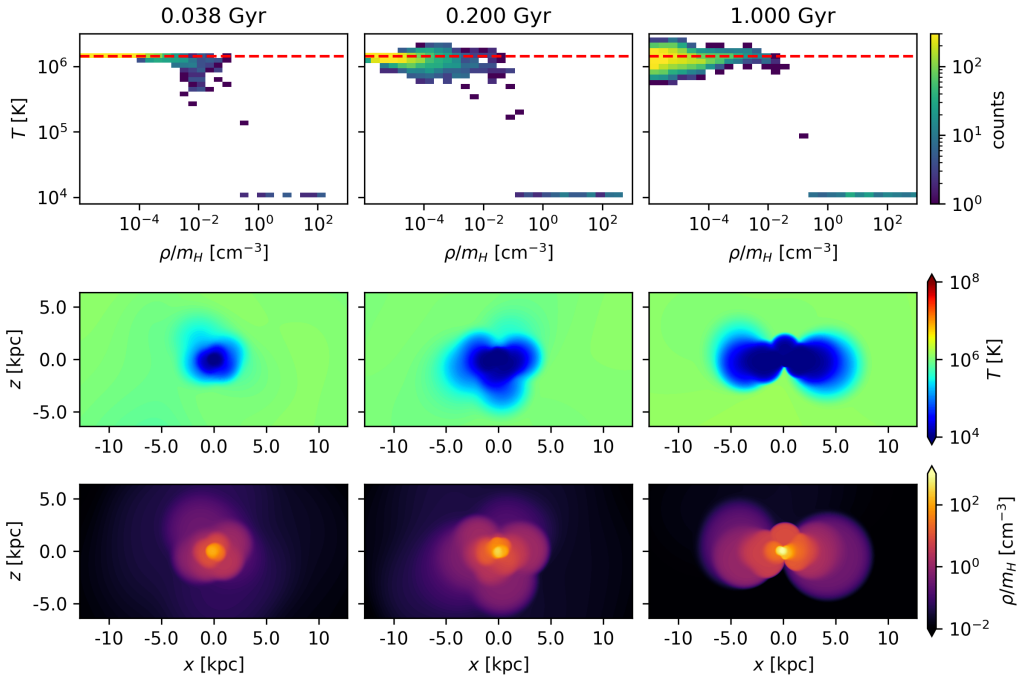

Figure 4.1: *Evolution of the cooling halo setup without magnetic fields. The upper panels show $T - \rho$ phase plots. The red line shows the initial temperature of all particles $T_{\mathrm{eq}} = 1.4 \times 10^6\,\mathrm{K}$. Cooling removes energy from the densest particle first, and their temperature quickly drops to the temperature floor $T_{min} = 10^4\,\mathrm{K}$. Middle panels show this temperature contrast in the maps of the $x - z$ slice through $y = 0$. The bottom panels show a density map – how a cooling halo forms a disk with a strong density contrast.*

Without cooling, the isothermal halo in isothermal potential will stay in equilibrium. With cooling, according to equation (4.7), dense central regions will quickly cool, and the centre will start to collapse and form a galactic disk. This is depicted in the Figure 4.1. The upper panels show the $T - \rho$ plot over time. The figure shows that the highest densities quickly

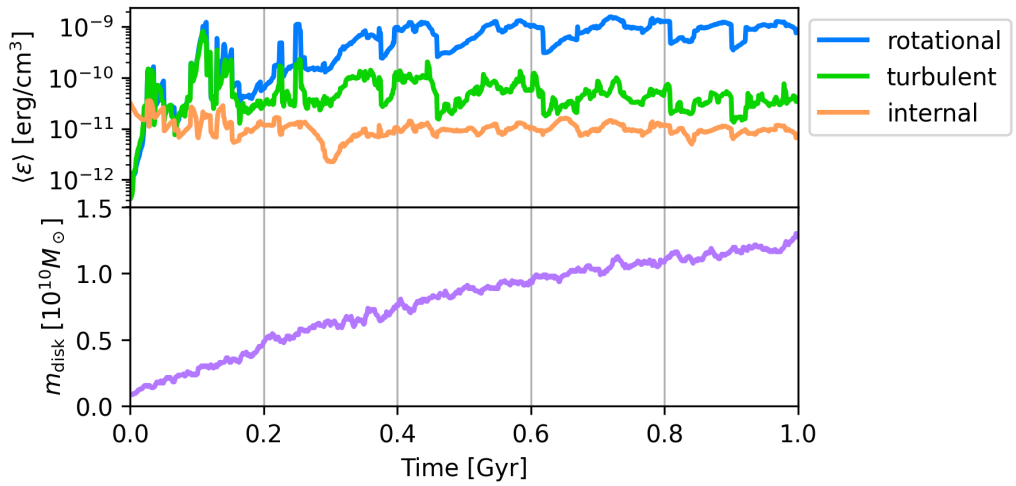

Figure 4.2: *Energy and collapsed mass inside the central disk with radius* $r = 10\,\mathrm{kpc}$ *and total height* $h = 1\,\mathrm{kpc}$ *in cooling halo simulation without magnetic fields. The first panel shows volume averaged internal, turbulent, and rotational energy densities over time. Rotational energy density is defined as* $\varepsilon_{\rm rot} = \rho v_\phi^2/2$, *turbulent –* $\varepsilon_{\rm turb} = \rho \delta v^2/2 \approx 3/2 \times \rho(v_z^2 + v_{r_\perp}^2)/2$. *The second panel shows the total mass inside a central disk that grows with time.*

cool and reach a minimal temperature of $T = 10^4\,\mathrm{K}$. After 1 Gyr, the number of cooled particles greatly increases along with maximum density. A similar picture is in the density and temperature maps on the same figure: the central region quickly cools down and starts to collapse, eventually forming a disk. Note a high density contrast between the disk and the halo.

We can also plot the time evolution of different energy densities and collapsed mass – Figure 4.2. The upper panel shows that initially, kinetic energy is subdominant, but over time, cooling removes internal energy, and kinetic energy starts to grow. Eventually, ordered rotation has ~ 20 times more energy than disordered turbulent motion and ~ 100 times more energy than internal. If we look at the total mass collapsed into the centre, it also prominently grows with time (see lower panel in Figure 4.2).

4.2.2 Isolated galaxy

The most prominent difference of this example from the cooling halo is that we run it with self-gravity, and it has initial density fluctuations. It leads to a formation of spiral arms and a central bulge – Figure 4.3. It will be important later since both spiral arms and bulge have stark density

Version of June 20, 2024– Created June 20, 2024 - 18:40

contrast with the rest of the disk.

Also, for the comparison with the MHD runs, let's plot internal, turbulent and rotational energies – this is done in Figure 4.4. You can see that rotational energy is 3 times higher than turbulent and 200 times higher than internal. Such high turbulence originates in the spiral arms.

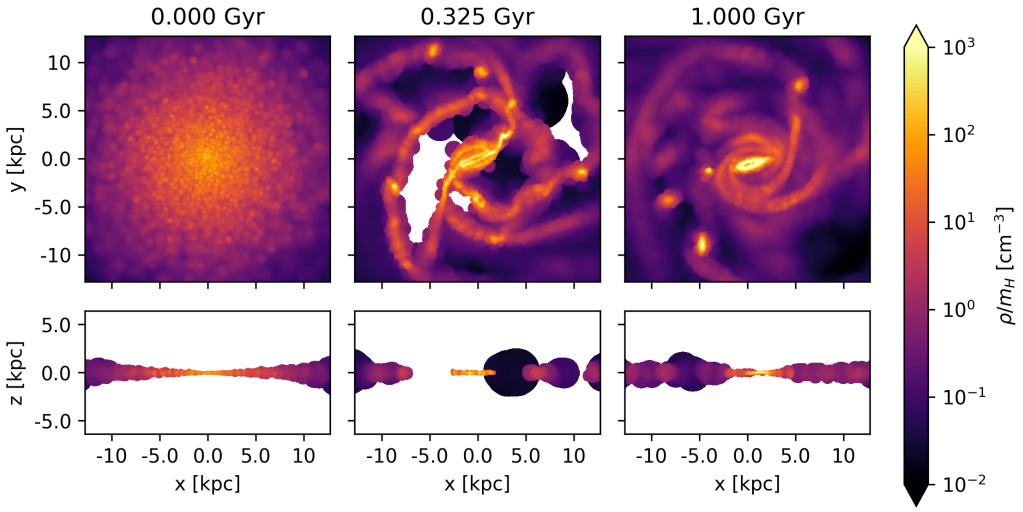

Figure 4.3: *Evolution of the isolated galaxy setup without magnetic fields. The upper panels show density maps in the x-y plane through $z = 0$. Lower panels show density maps in the x-z plane through $y = 0$. Note how initial density fluctuations with self-gravity lead to the formation of the spiral arms and central bulge with large density contrast.*

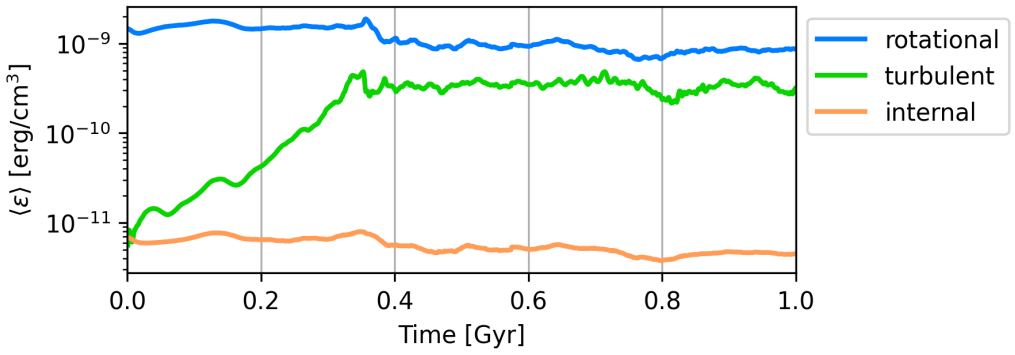

Figure 4.4: *Energy inside the central disk with radius $r = 10\,\mathrm{kpc}$ and total height $h = 1\,\mathrm{kpc}$ in isolated galaxy simulation without magnetic fields.*

4.3 Run with magnetic fields and "numerical explosion"

Starting from the very first runs of the described cooling halo setup, we had a problem with MHD that it "exploded". Here, I discuss this problem in more detail: what exactly happens and what we have tried to fix it.

4.3.1 How does explosion looks like

To understand what we mean by "explosion", look at the time evolution of the cooling halo with magnetic fields – Figure 4.5. Here is a timeline that this figure shows. Note that although specific values vary from run to run, the general behaviour of the explosion stays the same.

1. For the first 14 Myr, cooling removes internal energy from the central region; it starts to collapse, increasing the turbulent and rotational energy of the disk.

2. This collapse, however, also drives an increase in the divergence error. At 15 Myr it increases higher than 0.1.

3. 1 Myr later, when the error is large enough $\epsilon_{\mathrm{divB}} \gtrsim 0.5$, meaning that a significant fraction of magnetic field is unphysical, it drives a rapid increase in magnetic energy.

4. Magnetic energy stops to grow at approximate equipartition with internal/turbulent energy.

5. Later, at a random moment, high magnetic energy with high divergence error leads to the "numerical explosion". In this example, it happens at 38 Myr – internal and turbulent energies increase by two orders of magnitude over the 2 Myr.

6. After such enormous energy is released inside a central region, it rapidly expands, and mass inside the disk decreases almost to zero, as shown in the bottom left panel of Figure 4.5.

Every explosion consists of two nonphysical parts: first, divergence error grows to significant values and drives a jump in the magnetic field; second, high magnetic energy along with high divergence error drives the explosion itself, during which total energy is not conserved. These moments are illustrated as two vertical red lines on the left panel of Figure 4.5. The right panel of the figure shows maps at the moment of explosion

Version of June 20, 2024– Created June 20, 2024 - 18:40

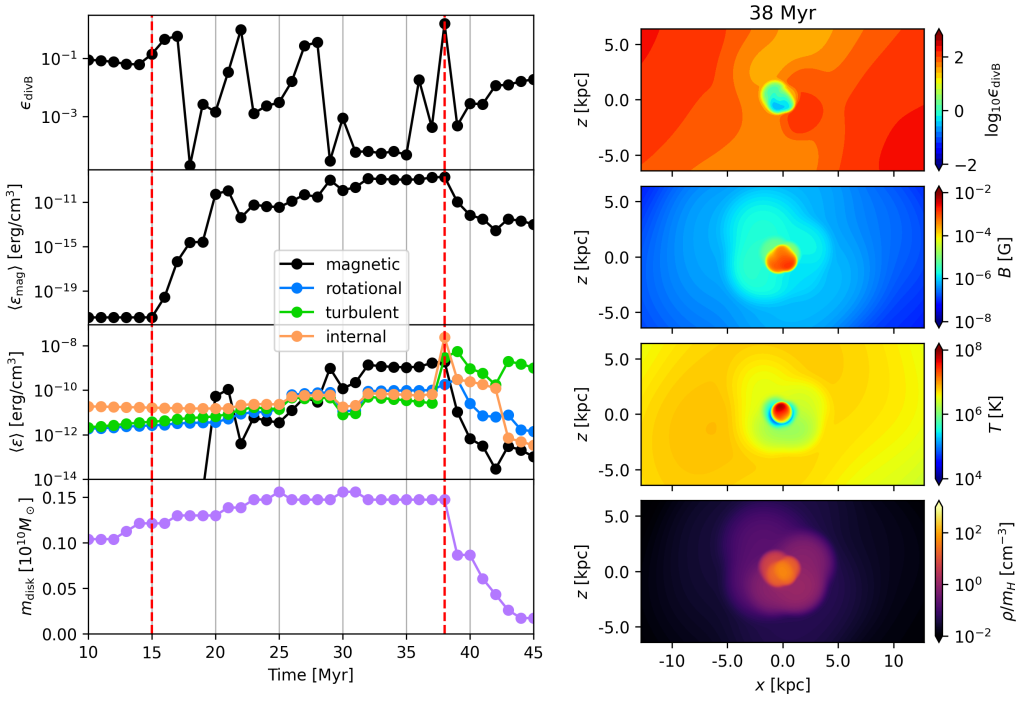

Figure 4.5: *The left half shows averaged parameters inside a disk of radius $r = 10\,\mathrm{kpc}$ and total height $h = 1\,\mathrm{kpc}$ in the cooling halo simulations with MHD. The top panel shows weighted by magnetic energy average divergence error as defined by (3.7). The second panel shows magnetic energy density. Third shows magnetic in comparison with rotational, turbulent, and internal energy densities. The bottom panel shows the total mass over time. Two vertical red lines note when ϵ_{divB} starts to increase and when internal and turbulent energies explode. The right half shows the central slice of the same setup in the x-z plane at the moment of the explosion $t = 38\,\mathrm{Myr}$. The top panel shows divergence error, second – magnetic field, third – temperature, and bottom – density. Compare these maps with the left column of Figure 4.1.*

$t = 38\,\mathrm{Myr}$. It teaches us a few important lessons: the dense central region has extremely high magnetic fields of $\sim 1000\,\mu\mathrm{G}$; the highest divergence error is not in the centre but in the underdense region around it; according to temperature map, the explosion happened in the central dense region, where the disk is starting to form.

To check whether disk formation is related to an explosion, we tried to remove cooling, increase the softening length of the gravitational potential ε, or increase temperature floor T_{min}. These three are requirements for the dense disk to form. If we significantly change any of them – there is no

disk and no explosion.

There are three reasons why the central disk is special in the cooling halo setup and can cause problems: disk has higher density – particles interact more, leading to problems accumulating quicker there; disk has severe density contrast with a halo – huge difference between nearby particles evolution can lead to problems on the surface; particles in the disk has high relative velocities due to the collapse – this leads to higher turbulence, stronger MHD interactions.

But which part of the code leads to an explosion, given special conditions in the centre? Our first suspicion fell on additional "tricks" in SPMHD: tensile correction, artificial resistivity, and divergence cleaning. Running with or without Dedner cleaning and tensile instabilities correction did not significantly change results. But running without artificial resistivity did! See Figure 4.6, which shows that there is no explosion in internal and turbulent energies. Instead, they stabilize at similar values to the run without MHD. Moreover, the magnetic field does not jump. It now takes reasonable 0.1 Gyr to reach approximate equipartition with internal and turbulent energies.

However, the divergence error still quickly reaches large values, meaning that results after $\sim$ 0.05 Gyr are significantly influenced by error and could be very wrong. Also, some of our tests and other authors suggest that artificial resistivity is crucial to capture discontinuities in the magnetic field correctly – an important feature for our setup with discontinuity between disk and halo. Therefore, turning it off is not a good solution and probably hints at a deeper issue in the simulation. Hence, we kept looking for another problem that may cause artificial diffusion to act unphysically.

For that, we wanted first to have a better intuition of what exactly causes the problem – higher density, density contrast, or gravitational collapse? To distinguish between these scenarios, we tried running another simulation setup – IsolatedGalaxy – it has already formed a disk with already high densities.

4.3.2 Isolated galaxy MHD runs

An isolated galaxy example also explodes in a very similar way to the cooling halo. The left panel of Figure 4.7 shows time evolution. First, spiral arms start to form, which leads to an increase in turbulent energy and the divergence error. It drives an increase in magnetic energy. Eventually, at some point when magnetic energy is already large, thermal and turbulent energy explodes.

Version of June 20, 2024– Created June 20, 2024 - 18:40

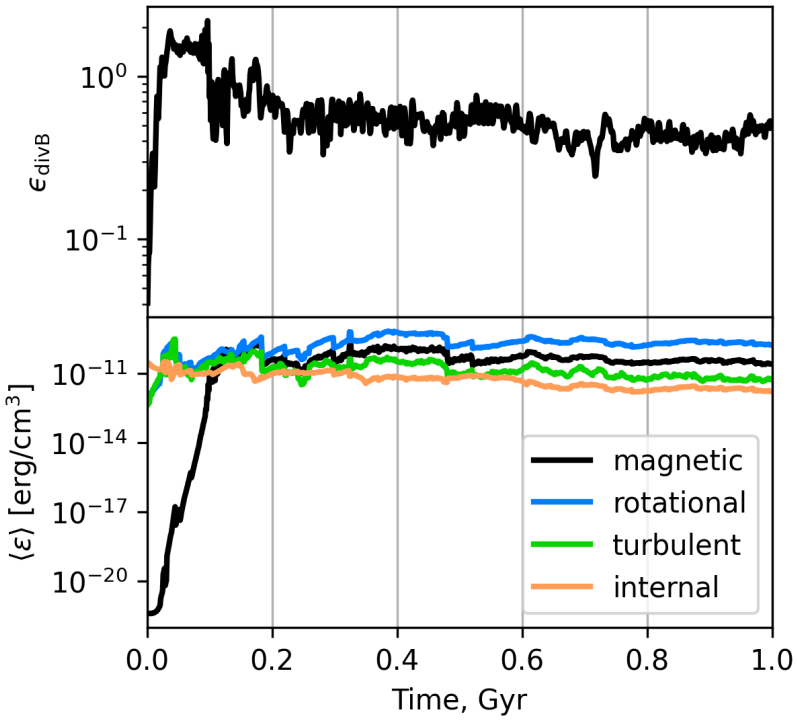

Figure 4.6: *Average divergence error (top) and energy densities (bottom) inside a disk of radius $r = 10\,\mathrm{kpc}$ and total height $h = 1\,\mathrm{kpc}$ in the cooling halo simulations with MHD, but without artificial diffusion. Notably, there is no explosion in this setup, and the magnetic field reaches equipartition in a reasonable time. Compare it with Figure 4.5.*

Let's also plot a map of how a galaxy looks like in the middle of an explosion $t = 0.325\,\mathrm{Gyr}$ – right panel of the Figure 4.7. Similarly to the cooling halo map (Figure 4.5), we see that the magnetic field is especially large in the densest regions, while divergence error is large in the underdense regions. This time, however, an explosion happens in the underdense regions between spiral arms.

Again, let's try running with some of the MHD tricks turned off. This time, turning on or off artificial resistivity does not change evolution and explosion. Turning off dedner also does not remove explosion, and neither does turning off tensile corrections. However, if we turn off both artificial resistivity and tensile corrections at once – there is no explosion! See Figure 4.8.

Comparing this example to the cooling halo, we conclude a few things:

first, the explosion is not related to the halo collapsing since it also happens in isolated galaxy examples; second, neither artificial diffusion nor tensile corrections are the problem themselves since different examples different combinations cause the explosion – the problem is more general, likely related to the high divergence error; third, from maps it follows that problems appear on the edge between different densities and are consequences of the high density contrast. In the cooling halo example, this is between the disk and the halo. In an isolated galaxy, it is between spiral arms or bulge and the rest of the galaxy.

Moreover, maps of the explosion in cooling halo and isolated galaxy examples suggest the following picture of how explosion happens:

1. Dense regions with high turbulence (either disk in cooling halo or spiral arms/bulge in the isolated galaxy) build up magnetic fields inside them along with small relative divergence error but high absolute divergence.

2. This error then propagates to the nearby underdense regions, for example, due to the Dedner cleaning scheme. Because of the strong density and magnetic field contrast, the resulting relative divergence error in the underdense regions is orders of magnitude higher and can reach $10^2 - 10^3$.

   Another possibility is why such high errors build up – underdense regions have higher time-step and are updated more rarely, which can lead to a divergence building up in them without its cleaning.

3. Eventually, such high divergence errors lead to an explosion in internal and turbulent energies. Explosion is always related to artificial diffusion, tensile corrections, or both. Artificial diffusion can transfer magnetic energy to internal, while tensile corrections can generate kinetic energy without conserving it. It is not necessarily a problem with those terms but rather a problem that appears at high divergence errors since they were not developed with such high errors in mind.

4.3.3 Unsuccessful ideas we tried to fix the explosion

- Since the problem is with dense regions, we tried turning on stars and star formation, hoping that all the problematic particles would be converted to stars. It did not happen, and it did not help.

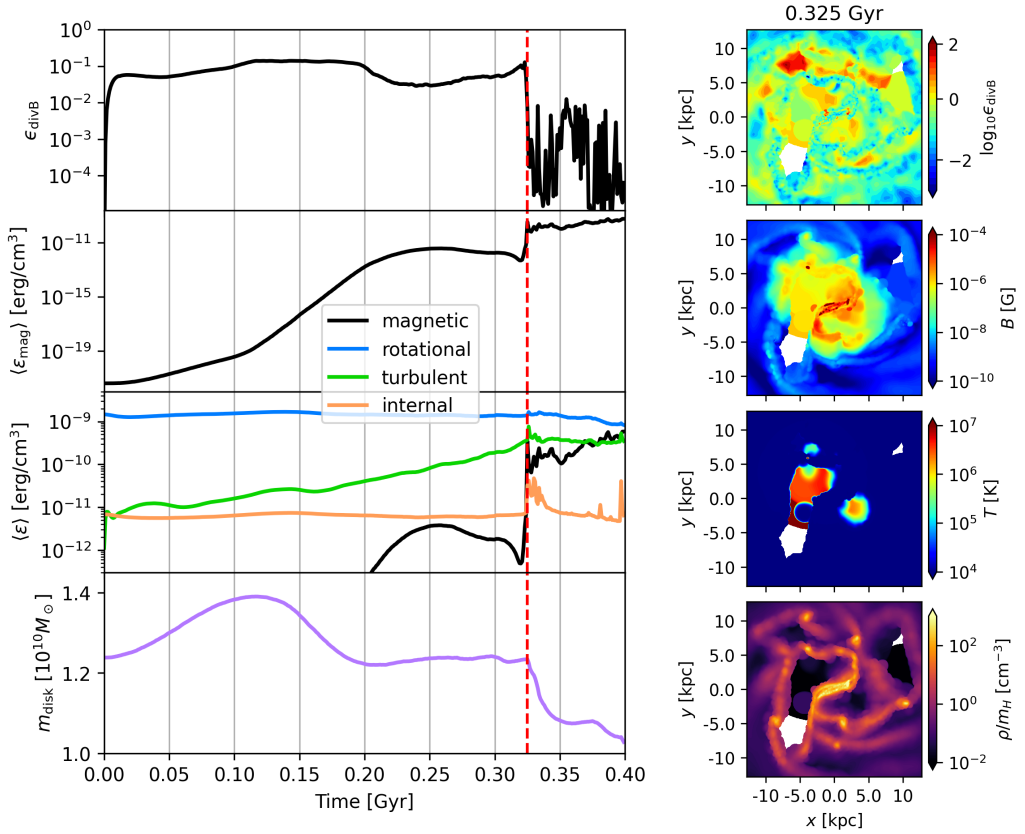

Figure 4.7: *Analog of Figure 4.5 for isolated galaxy with MHD run. The left half shows the time evolution of different parameters averaged inside a disk of radius $r = 10\,\mathrm{kpc}$ and total height $h = 1\,\mathrm{kpc}$. The vertical red line corresponds to a moment of explosion in internal and turbulent energies. This moment is plotted in detailed x-y maps on the right. Note the density contrast between spiral arms and regions between them. This density contrast leads to the build-up of huge divergence errors in the underdense regions and an explosion in internal/turbulent energies.*

- We tried to modify the cleaning speed and decay time in Dedner cleaning to improve its efficiency in removing errors. We were not able to find any modification that fixes the explosion.

- In some other tests, similar explosions were related to the machine precision errors and poorly selected units for magnetic fields. We tried running with different units, but it did not change the situation. For consistency, we run all the simulations now with the units that

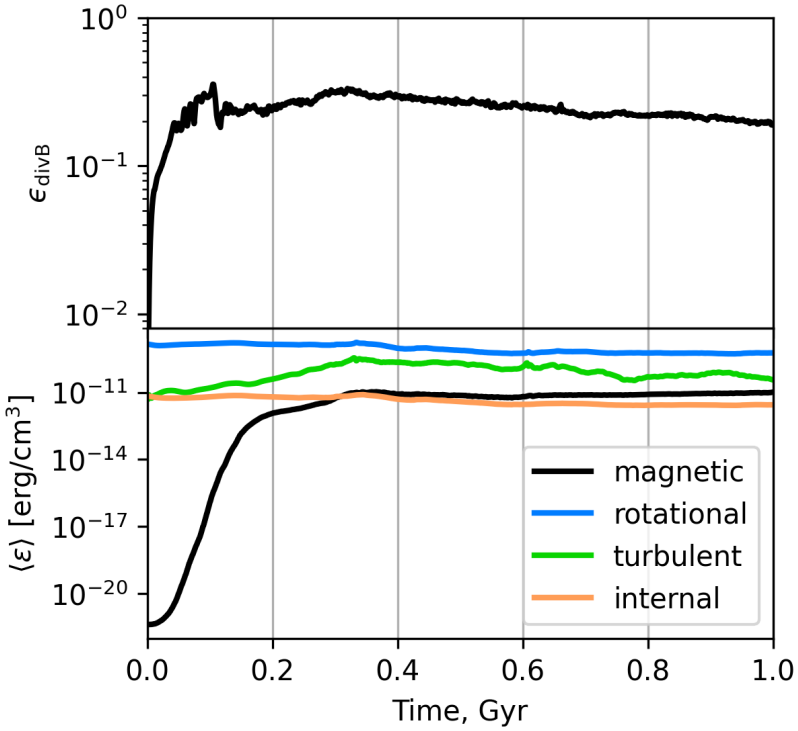

Figure 4.8: *Average divergence error (top) and energy densities (bottom) inside a disk of radius $r = 10\,\mathrm{kpc}$ and total height $h = 1\,\mathrm{kpc}$ in the isolated galaxy simulation with MHD, but without artificial diffusion and tensile corrections. Notably, there is no explosion in this setup, and the magnetic field reaches equipartition in a reasonable time. Compare it with Figure 4.7.*

proved to working correctly in other cosmological tests.

- At some point, we found a hint that it could be related to the time-stepping criterion. Therefore, we tried modifying an MHD time-step (3.8) by changing $\boldsymbol{\nabla} \cdot \boldsymbol{B}$ to different quantities. Ultimately, we tried to run with a minimum of three, additionally with a small 0.1 coefficient in front:

$$B_{\mathrm{factor}} = \max\left(\boldsymbol{\nabla} \cdot \boldsymbol{B},\ |\boldsymbol{\nabla} \times \boldsymbol{B}|,\ \frac{|\boldsymbol{B}|}{h}\right) \tag{4.11}$$

$$dt = 0.1 C_{\mathrm{CFL}} \sqrt{\frac{\mu_0 \rho}{B^2_{\mathrm{factor}}}}, \tag{4.12}$$

where CFL is a Courant-Friedrichs-Lewy coefficient used for other time-step criterions too. Still, it did not help, the explosion happened

again.

- Another hint that we noticed – explosion happens when there are particles that reach entropy or temperature floor. By testing different criteria and various cooling schemes, we found that this is just a coincidence – particles that reach the floor are also the densest particles in the simulation.

4.3.4 Temporary solutions to the explosion

Despite many tries without any clear solution, we found three ways to fix the explosion problem. Each, however, requires more computational resources and, thus, cannot be realistically implemented to all relevant setups and is only a temporary solution.

The first way is to lower the time-step for all particles. This could be done by lowering the CFL condition coefficient. Default value is $C_{\mathrm{CFL}} = 0.075$. We found that for isolated galaxy $C_{\mathrm{CFL}} = 0.005$ fixes the explosion, while for the cooling halo, slightly lower $C_{\mathrm{CFL}} = 0.001$ is required. It effectively increases the computational time by how much we reduce the time-step: $15 - 75$ times.

Another way – raising spatial resolution. For the cooling halo 10x increase from 7000 particles to 70000 particles with masses $8.7 \times 10^6\,\mathrm{M}_\odot$ fixed the problem. For isolated galaxies 6x increase in the number of particles (to 160000 gas particles with masses $1 \times 10^5\,\mathrm{M}_\odot$) helped in some of the runs, while others still had explosions. We did not have enough computational resources to try even higher resolution.

Finally, we found that limiting all the particles to have small and approximately the same time-step also stabilizes the run. We did it by setting a small maximal allowed time-step $1 \times 10^{-5}\,\mathrm{Gyr}$ in the simulation parameters. It suggests that the problem could be not in the density contrast per se but in a difference between time-steps in the dense and underdense regions. However, we discovered this fix only at the end of the project, so we have not tested it a lot.

We still do not know what exactly is the problem, but it is not unreasonable that lower time-step and higher resolution fixed them. Setting a lower time-step can help better resolve quickly changing values, for example, in the underdense region near the border with the dense disk or spiral arm. Higher spatial resolution helps resolve dense regions and the transition between dense and underdense regions.

Version of June 20, 2024– Created June 20, 2024 - 18:40

4.4 Dynamo or no dynamo

In all the previously discussed runs, there is a period of exponential growth of the magnetic fields that stops around equipartition with turbulent and internal energies. However, all those runs have high divergence errors; they are not consistent with each other and occasionally explode. The question remains whether this growth resembles physical or just a numerical nuisance. Some authors suggest that in our setup, there should be no dynamo [18], while others show dynamo in only slightly more complicated scenarios [23, 24, 30]. Given the fixes to the explosion and insights into what is causing all the troubles, let's now study dynamo in our setups more consistently.

4.4.1 More physical setup

First, let's add more physics to our setup to make it more realistic. Given the modular nature of SWIFT, this is very easy to do. Mostly we will rely on the subgrid model used by EAGLE [52, 53]. Here are the changes:

1. Instead of constant lambda cooling, we will use EAGLE cooling, which also has metalicity and temperature dependence of the cooling.

2. Instead of a constant temperature floor, we will use an EAGLE entropy floor, dependent on the density, to mimic real galaxies' interstellar medium temperature-density relation.

3. We add EAGLE star formation to our model: dense cold gas particles now may convert to stars at a realistic rate.

4. We add self-gravity also to the cooling halo setup.

To compare our results with the literature, we will slightly modify the parameters of our cooling halo setup to match the setup in the Pfrommer paper [30].

Halo parameters

1. $H = 67.7\,\mathrm{kms}^{-1}\mathrm{Mpc}^{-1}$, $\Omega_m = 0.3$, $\Omega_b = 0.047$, $X_{He} = 0.248$;

2. Isothermal potential: $v_{\mathrm{rot}} = 107.5\,\mathrm{km/s}$ (this corresponds to $M_{200} = 12\,\mathrm{M}_\odot$, $r_{200} = 315\,\mathrm{kpc}$, $T_{\mathrm{eq}} = 5.1 \times 10^5\,\mathrm{K}$) and softening length $\varepsilon = 1.0\,\mathrm{kpc}$;

Version of June 20, 2024– Created June 20, 2024 - 18:40

3. $\lambda = 0.3$;
4. $B_0 = 10^{-10}$ G along x-axis.

Finally, we adopt some changes in the numerical setup to avoid explosions. Namely, for the cooling halo, we increase the resolution from 2900 particles inside the virial radius to 10^5 and more particles. For the isolated galaxy, we will reduce the CFL constant to $C_{\mathrm{CFL}} = 0.005$ and also try to run higher resolution – with 6 times more particles.

4.4.2 Expected Behavior

In the cooling halo, we expect to see similar steps of galaxy formation to the ones discussed in the section 2.3:

1. First, cooling will quickly remove internal energy and associated pressure from the central region – it will collapse and form a disk.
2. During the collapse magnetic field will be amplified adiabatically (2.9): $B = B_0 \left(\frac{\rho}{\rho_0}\right)^{2/3}$.
3. Then, at some point, the dynamo will kick in and amplify the magnetic field up to equipartition levels.

4.4.3 Cooling halo results

Let's start by running a cooling halo with the setup discussed above (similar to Pfrommer et al. [30]) with 10^5 particles. The left panel of Figure 4.9 shows the resulting evolution of divergence error and energy densities inside the central disk. We see that even for this higher resolution, the divergence error grows up to ~ 1. Moreover, magnetic field behaviour is very jumpy. All this suggests that what we see is not a correctly resolved dynamo.

Again, the first suspicion falls onto the MHD tricks. This time, the cause was divergence cleaning. Without Dedner cleaning (the right panel of Figure 4.9), errors are smaller, and there is no dynamo! Figure 4.10 compares $B - \rho$ phase plots of two runs. While both have adiabatic contraption regime $B \sim \rho^{2/3}$ (see Equation. (2.9)), only run with Dedner has dynamo-like dense particles with high magnetic fields.

Errors without cleaning are still relatively large, so it is hard to say which behaviour is correct. To answer that question, I have tried running even higher resolution – 10^6 and 10^7 particles inside virial radius, both

Version of June 20, 2024– Created June 20, 2024 - 18:40

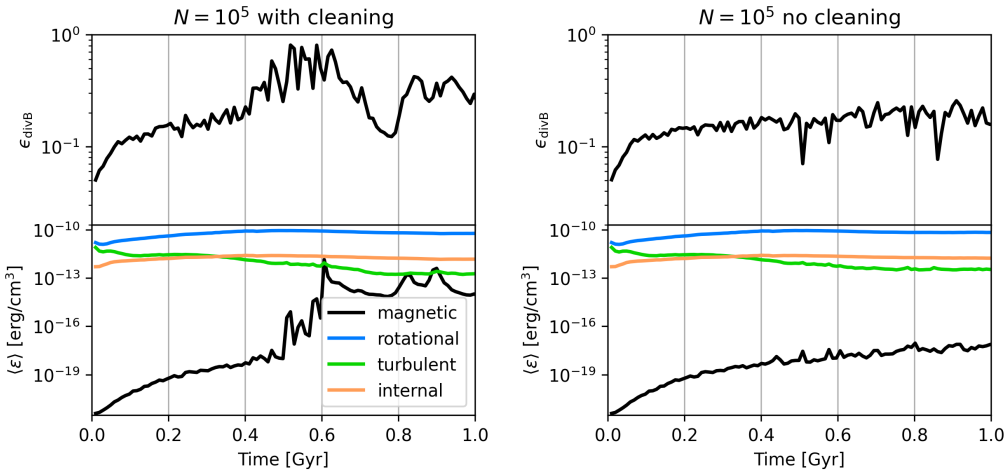

Figure 4.9: *Time evolution of the cooling halo with* 10^5 *gas particles inside virial radius with (left) and without (right) Dedner cleaning. All the values are averaged inside a disk of radius* $r = 10\,\mathrm{kpc}$ *and total height* $h = 1\,\mathrm{kpc}$*. Top panels show average divergence error, while lower panels show average magnetic, internal, turbulent, and rotational energy densities. With Dedner cleaning, there is a spurious dynamo, while there is none without Dedner cleaning.*

with Dedner cleaning. Respective plots are shown in the Figure 4.11. They show that while the 10^6 simulation still has a jump in divergence error and magnetic energy, the 10^7 run does not. Note that in some runs, even 10^7 particles were not enough, and there was a similar jump in divergence error with magnetic energy following it – this means that the behaviour is very susceptible to numerical errors.

These results suggest that the correct behaviour in our cooling halo setup is without a dynamo. This agrees with [18]. They also show that there should be no dynamo in runs without stellar feedback.

Also, this means that all the exponential increases in magnetic energy we have seen for this setup before – were spurious. Moreover, it suggests that Dedner cleaning for lower resolutions makes simulation even worse than without it – not only does it increase an error, but it also introduces spurious dynamo.

Why does Dedner cleaning make things even worse? The answer is probably lying again in the harsh density contrast. During the collapse, the central disk gets a high magnetic field B_{disk} and, along with it, a small relative divergence error $\sim 10^{-2}$. Absolute values of divergence are still

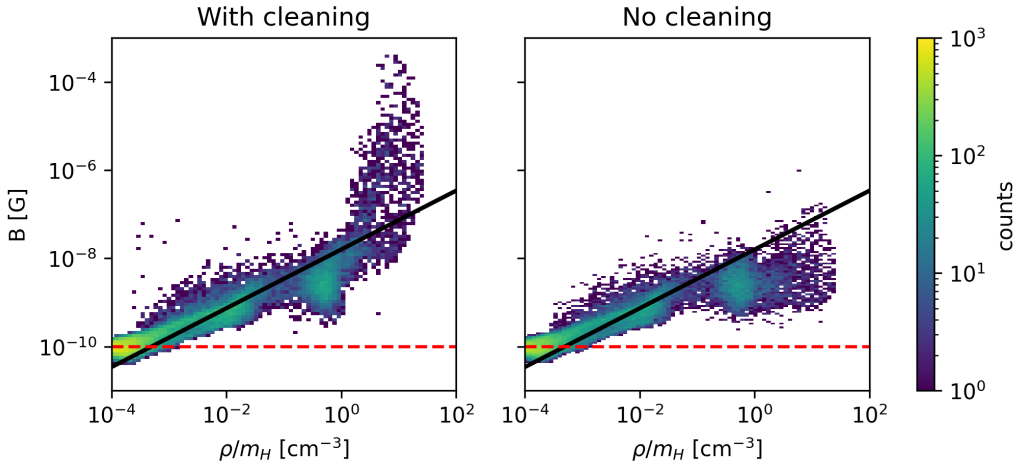

Figure 4.10: *Phase plots $B - \rho$ of the cooling halo with (left) and without (right) Dedner cleaning at $t = 0.61\,\mathrm{Gyr}$. The seed magnetic field is noted by the red dashed line. With cleaning, there is a population of high-density particles with increased magnetic fields – they correspond to a spurious dynamo. Without Dedner cleaning, the only increase in magnetic field is due to adiabatic contraption, and it follows $B \sim \rho^{2/3}$ (black line), as predicted from flux freezing* (2.9).

high

$$\boldsymbol{\nabla} \cdot \boldsymbol{B} \sim 10^{-2} \frac{B_{\mathrm{disk}}}{h_{\mathrm{disk}}},$$

where $h_{\mathrm{disk}} \sim (\rho_{\mathrm{disk}})^{-1/3}$ is typical distance between particles in the disk. Dedner scalar effectively propagates this high absolute divergence into nearby halo particles according to equation (3.3). Halo has lower density and lower magnetic fields, which leads to a huge relative divergence error:

$$\epsilon_{\mathrm{divB,halo}} = \frac{h_{\mathrm{halo}} \boldsymbol{\nabla} \cdot \boldsymbol{B}}{B_{\mathrm{halo}}} \sim 10^{-2} \frac{h_{\mathrm{halo}} B_{\mathrm{disk}}}{h_{\mathrm{disk}} B_{\mathrm{halo}}} \approx 10^{-2} \frac{B_{\mathrm{disk}}}{B_{\mathrm{halo}}} \left(\frac{\rho_{\mathrm{disk}}}{\rho_{\mathrm{halo}}} \right)^{1/3}.$$

From Figure 4.10, we see that magnetic field can be different by ~ 4 orders of magnitude between disk (high densities) and halo (low densities) while maps like Figure 4.1 show a few orders of magnitude difference in densities. From the estimate above, divergence errors in the halo should be huge $\epsilon_{\mathrm{divB,halo}} \sim 10^2 - 10^3$. And indeed, we observe such errors, for example, on the maps 4.5.

The whole MHD scheme was not developed to work correctly under such large errors. This can lead to a spurious increase in the magnetic

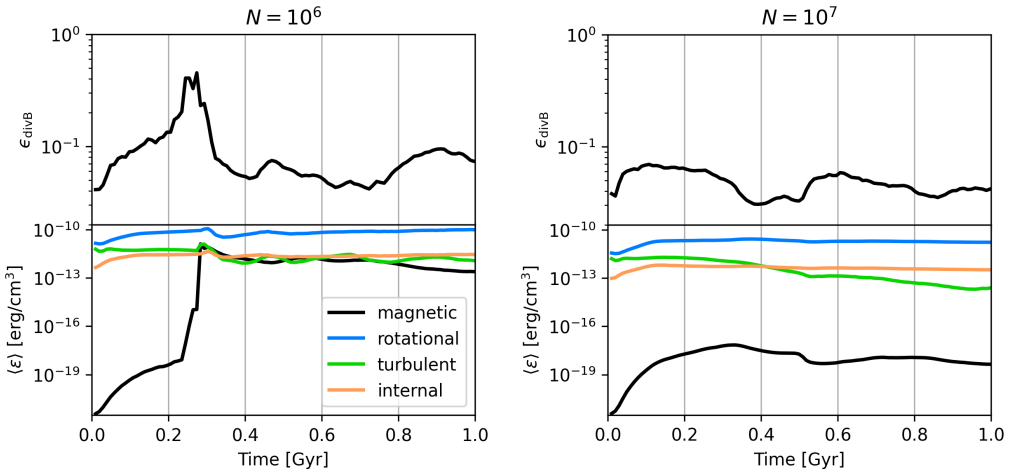

Figure 4.11: *Time evolution of the cooling halo with* 10^6 *(left) and* 10^7 *(right) gas particles inside virial radius with Dedner cleaning. All the values are averaged inside a disk of radius* $r = 10\,\mathrm{kpc}$ *and total height* $h = 1\,\mathrm{kpc}$*. Top panels show average divergence error, while lower panels show average magnetic, internal, turbulent, and rotational energy densities. After reaching a high enough resolution (*10^7 *in this case), the spurious dynamo disappears.*

field that eventually leaks back to the disk and influences it even more, repeating the cycle.

Instead of increasing resolution, another thing that we tried was changing the time-step. Setting a lower CFL coefficient (i.e. decreasing time-step by a constant factor everywhere) did not help – Dedner cleaning still produces spurious dynamo. We also tried to set small time-step everywhere. And indeed – it helped to fix the problem, now with Dedner cleaning there is also no dynamo. This suggests that the problem might be because of the time-step difference inside and outside of the disk, but more tests are needed to be sure.

4.4.4 Isolated galaxy results

Now, let's repeat this exercise for the isolated galaxy. We start with the same initial conditions as in the explosion examples, but now with all the additional physics and lower CFL to avoid explosions. Figure 4.12 shows evolution with time. This time, both with and without a Dedner cleaning, we see a smooth increase in magnetic energy over reasonable 0.1 Gyr that stops around equipartition with internal and turbulent.

Version of June 20, 2024– Created June 20, 2024 - 18:40

To answer whether this is a spurious dynamo, we plot disk maps after the magnetic field increased – Figure 4.13. The magnetic energy of the disk is concentrated in the central blob. A similar picture was obtained by [22] in the Powell cleaning scheme. They compared it to the same simulation with constraint transport and concluded that this blob was an artefact of the cleaning scheme. The correct magnetic field should follow the spiral arms and not concentrate in the centre. This does not necessarily imply that the dynamo itself is an artefact, but the exact mechanism of how it occurs may not be entirely correct.

Finally, we tried running 6 times higher resolution – see Figure 4.14. Again, there is no dynamo! Note, however, that in different runs with the same resolution, we sometimes see a dynamo. This means that this resolution is not enough to fully resolve the setup, and it is susceptible to numerical errors.

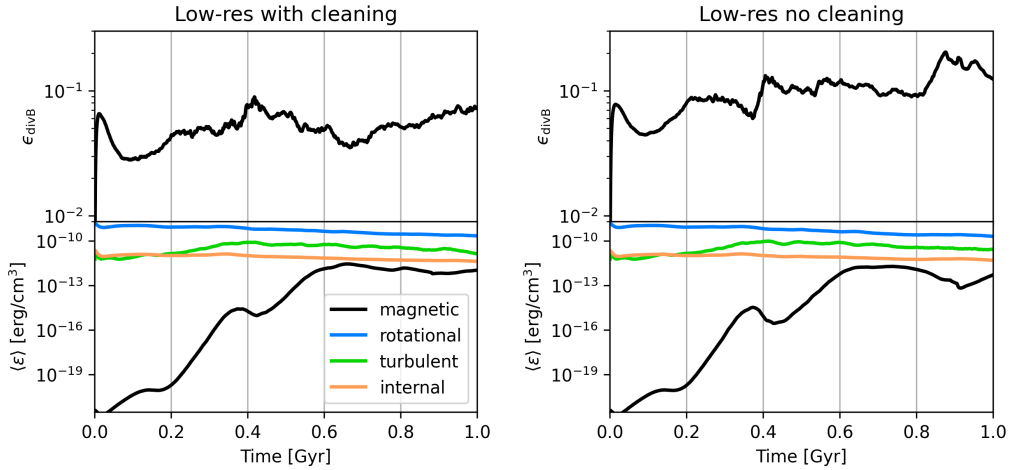

Figure 4.12: *Time evolution of the isolated galaxy inside virial radius with (left) and without (right) Dedner cleaning. All the values are averaged inside a disk of radius $r = 10\,\mathrm{kpc}$ and total height $h = 1\,\mathrm{kpc}$. Top panels show average divergence error, while lower panels show average magnetic, internal, turbulent, and rotational energy densities. Note that this time dynamo is present in both cases.*

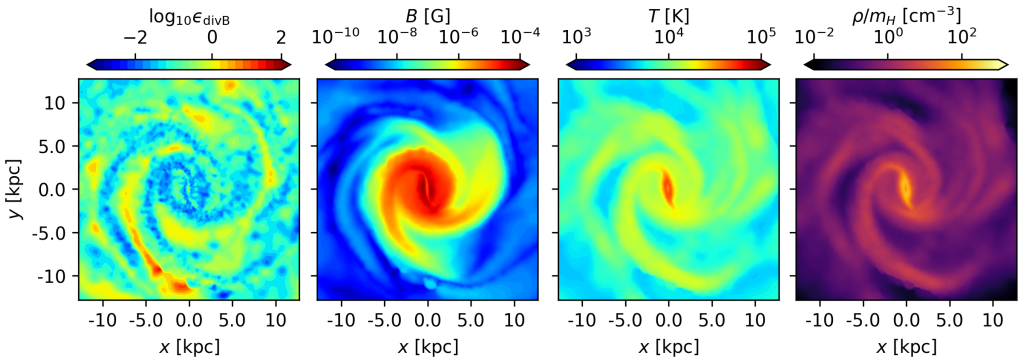

Figure 4.13: *Maps of the isolated galaxy with MHD in the $x - y$ plane after the dynamo at $t = 0.6\,\mathrm{Gyr}$. From left to right: divergence error, magnetic field, temperature, density. Note the numerical artefact in the magnetic field in the centre of the disk.*

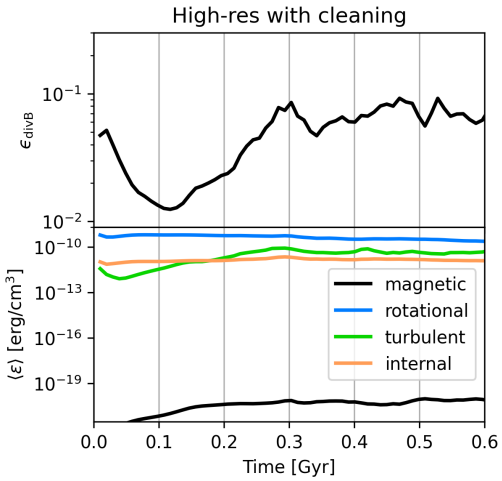

Figure 4.14: *Time evolution of the isolated galaxy inside virial radius with Dedner cleaning. All the values are averaged inside a disk of radius $r = 10\,\mathrm{kpc}$ and total height $h = 1\,\mathrm{kpc}$. Top panels show average divergence error, while lower panels show average magnetic, internal, turbulent, and rotational energy densities. Note that this plot stops earlier than others – this is simply because of the high computational cost of this run.*

Version of June 20, 2024– Created June 20, 2024 - 18:40

Chapter 5

Summary and conclusions

In this work, we for the first time studied magnetic fields during galaxy formation using the SWIFT code. The SPMHD module was developed only recently by Orestis Karapiperis et al. and was mostly tested in standard specialized setups. Here, we tried to apply it to a more realistic setup – isothermal gas halo inside dark matter potential that cools and starts to form a galactic disk in the centre.

Our main conclusion is that the current implementation of SPMHD struggles with correctly resolving the cooling halo setup.

As was shown in section 4.3, the most problematic for the simulation is the density contrast between the forming disk and the halo around it.

Dedner cleaning struggles to keep divergence errors low. Moreover, in some runs, divergence cleaning is the reason for the spurious dynamo – likely because it effectively propagates high divergence from dense disk to nearby underdense halo particles, making their relative divergence error as high as $10^3 - 10^4$. Such high error causes a magnetic field to grow and leak back to the disk, repeating the cycle.

High divergence errors can also cause troubles in other parts of the code – with artificial diffusion and tensile corrections. Artificial diffusion can transfer magnetic field energy into thermal, while tensile corrections do not conserve energy and can generate kinetic energy. With extreme divergence errors, these terms can behave very wrong and create a "numerical explosion" in internal and turbulent energies.

We have not found any satisfactory way to fix those problems, but higher spatial and temporal resolution can help.

Reducing the time-step for all particles by a factor of $15 - 75$ compared to the default one helps to fix explosion, but not spurious dynamo. However, if we keep the time-step of all particles low and almost the same –

smaller than 1×10^{-5} Gyr, both spurious dynamo and explosion disappear.

Having a mass resolution smaller than 10^4 to $10^5\,M_\odot$ also helps to fix spurious dynamo.

In the high-resolution (spatial and/or temporal) runs, we found that in our setup, there is no dynamo. It is consistent with some of the other simulation papers [18]. It is believed that the main driver of the small-scale dynamo in galaxies is turbulence generated from supernova explosions. Since we do not include stellar feedback in our model, we indeed should not see any dynamo. The exponential increase in magnetic fields we have seen in some runs is thus only a numerical artefact.

5.1 Next steps

We conclude by listing ideas for future research relevant to our findings.

In this work, we focused a lot on trying to fix the "numerical explosion". However, I do not think it is itself a problem that needs fixing, but rather a symptom – a symptom of a very high divergence error that breaks the whole scheme, leading to an explosion. Therefore, the main focus for future works should be on keeping the divergence error reasonably small.

1. **Finding a simpler setup with the same problems**

   In the cooling halo and isolated galaxy, all the problems seem to arise because of the high density contrast. Perhaps there is a simpler and more standard setup that also has density contrast and will have the same kind of problems. If so, finding and testing it will give a clearer picture of the issue.

2. **Better time-step limiter near the density contrast**

   Currently, the best lead we have is that lowering time-steps for all particles to the same value helps to keep the divergence error low, to avoid spurious dynamo and numerical explosion. This suggests that the problem could be not in the density contrast per se, but in the "time-step contrast". Because halo has much less density, time-step in it will be higher, therefore particles will be updated less frequently. Perhaps, this can lead to problems with Dedner cleaning.

   One first needs to test whether indeed the problem is in a time-step difference between disk and halo. For example, by setting coordinate-dependent time-step criterion that is limited to small values near the

disk. If it helps, one can then come up with a smarter time-step limiter, that lights up only when particle has a neighbour with much higher density.

3. **Artificial Dedner conduction**

   If time-step idea will not be sufficient, one can think about improving Dedner cleaning scheme to work even in high density contrast. Perhaps one can come up with a similar to the artificial conduction term but for the Dedner scalar, to better capture its discontinuities between disk and halo.

4. **Testing stellar feedback role in dynamos**

   Finally, once the high divergence error problem is fixed, one should run the same setups with and without stellar feedback. This will help to confirm or disprove our conclusion – that a dynamo occurs only with feedback and not without it.

Bibliography

[1] Mark Vogelsberger, Federico Marinacci, Paul Torrey, and Ewald Puchwein. Cosmological simulations of galaxy formation. *Nature Reviews Physics*, 2(1):42–66, 2020.

[2] Axel Brandenburg and Evangelia Ntormousi. Galactic Dynamos. *Annual Review of Astronomy and Astrophysics*, 61(Volume 61, 2023):561–606, August 2023. Publisher: Annual Reviews.

[3] Axel Brandenburg and Kandaswamy Subramanian. Astrophysical magnetic fields and nonlinear dynamo theory. *Physics Reports*, 417(1):1–209, October 2005.

[4] Anvar Shukurov and Kandaswamy Subramanian. *Astrophysical Magnetic Fields: From Galaxies to the Early Universe*. Cambridge Astrophysics. Cambridge University Press, 2021.

[5] Rainer Beck. Magnetic fields in spiral galaxies. *The Astronomy and Astrophysics Review*, 24(1):4, December 2015.

[6] Rainer Beck and Marita Krause. Revised equipartition & minimum energy formula for magnetic field strength estimates from radio synchrotron observations. *Astron. Nachr.*, 326:414–427, 2005.

[7] DD Sokoloff, AA Bykov, A Shukurov, EM Berkhuijsen, R Beck, and AD Poezd. Depolarization and faraday effects in galaxies. *Monthly Notices of the Royal Astronomical Society*, 299(1):189–206, 1998.

[8] Roger H Hildebrand, Larry Kirby, Jessie L Dotson, Martin Houde, and John E Vaillancourt. Dispersion of magnetic fields in molecular clouds. i. *The Astrophysical Journal*, 696(1):567, 2009.

[9] Richard M Crutcher, Benjamin Wandelt, Carl Heiles, Edith Falgarone, and Thomas H Troland. Magnetic fields in interstellar clouds from zeeman observations: inference of total field strengths by bayesian analysis. *The Astrophysical Journal*, 725(1):466, 2010.

[10] Andrew Fletcher. Magnetic fields in nearby galaxies. *arXiv preprint arXiv:1104.2427*, 2011.

[11] B Adebahr, M Krause, U Klein, Marek Weżgowiec, DJ Bomans, and R-J Dettmar. M 82–a radio continuum and polarisation study-i. data reduction and cosmic ray propagation. *Astronomy & Astrophysics*, 555:A23, 2013.

[12] Rainer Beck. Magnetic fields in the nearby spiral galaxy ic 342: A multi-frequency radio polarization study. *Astronomy & Astrophysics*, 578:A93, 2015.

[13] JH Piddington. The magnetic fields and radio emission of galaxies. *Monthly Notices of the Royal Astronomical Society*, 128(4):345–359, 1964.

[14] Tosio Ôki, Mitsuaki Fujimoto, and Zyuiti Hitotuyanagi. Part iii. formation of spiral arms and dynamical model of barred galaxies. *Progress of Theoretical Physics Supplement*, 31:77–115, 1964.

[15] P Frick, R Stepanov, A Shukurov, and D Sokoloff. Structures in the rotation measure sky. *Monthly Notices of the Royal Astronomical Society*, 325(2):649–664, 2001.

[16] CL Van Eck, JC Brown, Anvar Shukurov, and Andrew Fletcher. Magnetic fields in a sample of nearby spiral galaxies. *The Astrophysical Journal*, 799(1):35, 2015.

[17] FS Tabatabaei, E Schinnerer, EJ Murphy, R Beck, B Groves, S Meidt, M Krause, H-W Rix, K Sandstrom, AF Crocker, et al. A detailed study of the radio-fir correlation in ngc 6946 with herschel-pacs/spire from kingfish. *Astronomy & Astrophysics*, 552:A19, 2013.

[18] Michael Rieder and Romain Teyssier. A small-scale dynamo in feedback-dominated galaxies as the origin of cosmic magnetic fields - I. The kinematic phase. *Monthly Notices of the Royal Astronomical Society*, 457(2):1722–1738, April 2016.

[19] Charles R Evans and John F Hawley. Simulation of magnetohydrodynamic flows-a constrained transport method. *Astrophysical Journal,*

Part 1 (ISSN 0004-637X), vol. 332, Sept. 15, 1988, p. 659-677., 332:659–677, 1988.

[20] Kenneth G Powell, Philip L Roe, Timur J Linde, Tamas I Gombosi, and Darren L De Zeeuw. A solution-adaptive upwind scheme for ideal magnetohydrodynamics. *Journal of Computational Physics*, 154(2):284–309, 1999.

[21] Andreas Dedner, Friedemann Kemm, Dietmar Kröner, C-D Munz, Thomas Schnitzer, and Matthias Wesenberg. Hyperbolic divergence cleaning for the mhd equations. *Journal of Computational Physics*, 175(2):645–673, 2002.

[22] Philip Mocz, Rüdiger Pakmor, Volker Springel, Mark Vogelsberger, Federico Marinacci, and Lars Hernquist. A moving mesh unstaggered constrained transport scheme for magnetohydrodynamics. *Monthly Notices of the Royal Astronomical Society*, 463(1):477–488, 2016.

[23] Alexander M Beck, Harald Lesch, Klaus Dolag, Hanna Kotarba, Annette Geng, and Federico A Stasyszyn. Origin of strong magnetic fields in milky way-like galactic haloes. *Monthly Notices of the Royal Astronomical Society*, 422(3):2152–2163, 2012.

[24] Rüdiger Pakmor and Volker Springel. Simulations of magnetic fields in isolated disc galaxies. *Monthly Notices of the Royal Astronomical Society*, 432(1):176–193, 2013.

[25] Oliver Gressel, Detlef Elstner, Udo Ziegler, and Günther Rüdiger. Direct simulations of a supernova-driven galactic dynamo. *Astronomy & Astrophysics*, 486(3):L35–L38, 2008.

[26] Evangelia Ntormousi, Konstantinos Tassis, Fabio Del Sordo, Francesca Fragkoudi, and Rüdiger Pakmor. A dynamo amplifying the magnetic field of a milky-way-like galaxy. *Astronomy & Astrophysics*, 641:A165, 2020.

[27] Peng Wang and Tom Abel. Magnetohydrodynamic simulations of disk galaxy formation: the magnetization of the cold and warm medium. *The Astrophysical Journal*, 696(1):96, 2009.

[28] Yohan Dubois and Romain Teyssier. Magnetised winds in dwarf galaxies. *Astronomy & Astrophysics*, 523:A72, 2010.

[29] Frederick A Gent, Mordecai-Mark Mac Low, Maarit J Käpylä, and Nishant K Singh. Small-scale dynamo in supernova-driven interstellar turbulence. *The Astrophysical Journal Letters*, 910(2):L15, 2021.

[30] Christoph Pfrommer, Maria Werhahn, Rudiger Pakmor, Philipp Girichidis, and Christine M. Simpson. Simulating radio synchrotron emission in star-forming galaxies: small-scale magnetic dynamo and the origin of the far-infrared-radio correlation. *Monthly Notices of the Royal Astronomical Society*, 515:4229–4264, September 2022. ADS Bibcode: 2022MNRAS.515.4229P.

[31] Michael Rieder and Romain Teyssier. A small-scale dynamo in feedback-dominated galaxies - II. The saturation phase and the final magnetic configuration. *Monthly Notices of the Royal Astronomical Society*, 471(3):2674–2686, November 2017.

[32] Eugene N Parker. Hydromagnetic dynamo models. *Astrophysical Journal, vol. 122, p. 293*, 122:293, 1955.

[33] George Backus. A class of self-sustaining dissipative spherical dynamos. *Annals of Physics*, 4(4):372–447, 1958.

[34] Alfred Herzenberg. Geomagnetic dynamos. *Philosophical Transactions of the Royal Society of London. Series A, Mathematical and Physical Sciences*, 250(986):543–583, 1958.

[35] Gareth Owen Roberts. Dynamo action of fluid motions with two-dimensional periodicity. *Philosophical Transactions of the Royal Society of London. Series A, Mathematical and Physical Sciences*, 271(1216):411–454, 1972.

[36] FJ Lowes and I Wilkinson. Geomagnetic dynamo: a laboratory model. *Nature*, 198(4886):1158–1160, 1963.

[37] Thomas George Cowling. The magnetic field of sunspots. *Monthly Notices of the Royal Astronomical Society, Vol. 94, p. 39-48*, 94:39–48, 1933.

[38] AP Kazantsev. Enhancement of a magnetic field by a conducting fluid. *Sov. Phys. JETP*, 26(5):1031–1034, 1968.

[39] K Ferriere. Alpha-tensor and diffusivity tensor due to supernovae and superbubbles in the galactic disk near the sun. *Astronomy and Astrophysics, v. 310, p. 438-455*, 310:438–455, 1996.

[40] Dominik RG Schleicher, Robi Banerjee, Sharanya Sur, Tigran G Arshakian, Ralf S Klessen, Rainer Beck, and Marco Spaans. Small-scale dynamo action during the formation of the first stars and galaxies-i. the ideal mhd limit. *Astronomy & Astrophysics*, 522:A115, 2010.

[41] David J. Stevenson. Lecture notes: Planetary structure and evolution, 2024. `https://web.gps.caltech.edu/classes/ge131/notes2024/Chapter_22.pdf`.

[42] Ludwig Biermann. Über den ursprung der magnetfelder auf sternen und im interstellaren raum (miteinem anhang von a. schlüter). *Zeitschrift Naturforschung Teil A*, 5:65, 1950.

[43] Matthieu Schaller et al. SWIFT: A modern highly-parallel gravity and smoothed particle hydrodynamics solver for astrophysical and cosmological applications. *Monthly Notices of the Royal Astronomical Society*, 530(2):2378–2419, May 2024.

[44] Holger Wendland. Piecewise polynomial, positive definite and compactly supported radial functions of minimal degree. *Advances in computational Mathematics*, 4:389–396, 1995.

[45] Josh Borrow, Matthieu Schaller, Richard G. Bower, and Joop Schaye. SPHENIX: smoothed particle hydrodynamics for the next generation of galaxy formation simulations. *Monthly Notices of the Royal Astronomical Society*, 511(2):2367–2389, April 2022.

[46] Fabrice Durier and Claudio Dalla Vecchia. Implementation of feedback in smoothed particle hydrodynamics: towards concordance of methods. *Monthly Notices of the Royal Astronomical Society*, 419(1):465–478, January 2012.

[47] GJ Phillips and JJ Monaghan. A numerical method for three-dimensional simulations of collapsing, isothermal, magnetic gas clouds. *Monthly Notices of the Royal Astronomical Society (ISSN 0035-8711), vol. 216, Oct. 15, 1985, p. 883-895.*, 216:883–895, 1985.

[48] Daniel J. Price, James Wurster, Terrence S. Tricco, Chris Nixon, StÃ©ven Toupin, Alex Pettitt, Conrad Chan, Daniel Mentiplay, Guillaume Laibe, Simon Glover, Clare Dobbs, Rebecca Nealon, David Liptai, Hauke Worpel, ClÃ©ment Bonnerot, Giovanni Dipierro, Giulia Ballabio, Enrico Ragusa, Christoph Federrath, Roberto Iaconi, Thomas Reichardt, Duncan Forgan, Mark Hutchison, Thomas Constantino, Ben Ayliffe, Kieran Hirsh, and Giuseppe Lodato. Phantom:

A Smoothed Particle Hydrodynamics and Magnetohydrodynamics Code for Astrophysics. *Publications of the Astronomical Society of Australia*, 35:e031, September 2018. ADS Bibcode: 2018PASA...35...31P.

[49] Terrence S Tricco and Daniel J Price. Constrained hyperbolic divergence cleaning for smoothed particle magnetohydrodynamics. *Journal of Computational Physics*, 231(21):7214–7236, 2012.

[50] Terrence S Tricco, Daniel J Price, and Matthew R Bate. Constrained hyperbolic divergence cleaning in smoothed particle magnetohydrodynamics with variable cleaning speeds. *Journal of Computational Physics*, 322:326–344, 2016.

[51] RÃŒdiger Pakmor, Federico Marinacci, and Volker Springel. MAGNETIC FIELDS IN COSMOLOGICAL SIMULATIONS OF DISK GALAXIES. *The Astrophysical Journal Letters*, 783(1):L20, February 2014. Publisher: The American Astronomical Society.

[52] Joop Schaye, Robert A. Crain, Richard G. Bower, Michelle Furlong, Matthieu Schaller, Tom Theuns, Claudio Dalla Vecchia, Carlos S. Frenk, I. G. McCarthy, John C. Helly, Adrian Jenkins, Y. M. Rosas-Guevara, Simon D. M. White, Maarten Baes, C. M. Booth, Peter Camps, Julio F. Navarro, Yan Qu, Alireza Rahmati, Till Sawala, Peter A. Thomas, and James Trayford. The EAGLE project: simulating the evolution and assembly of galaxies and their environments. *Monthly Notices of the Royal Astronomical Society*, 446(1):521–554, January 2015.

[53] Robert A. Crain, Joop Schaye, Richard G. Bower, Michelle Furlong, Matthieu Schaller, Tom Theuns, Claudio Dalla Vecchia, Carlos S. Frenk, Ian G. McCarthy, John C. Helly, Adrian Jenkins, Yetli M. Rosas-Guevara, Simon D. M. White, and James W. Trayford. The EAGLE simulations of galaxy formation: calibration of subgrid physics and model variations. *Monthly Notices of the Royal Astronomical Society*, 450(2):1937–1961, June 2015.